

Electron Microprobe Analysis by Wavelength Dispersive X-ray Spectrometry on the JEOL JXA-733 Superprobe

(IAP 2003: Course 12.141)

Course Notes

The electron microprobe provides a complete micron-scale quantitative chemical analysis of inorganic solids. The method is nondestructive and utilizes characteristic x-rays excited by an electron beam, incident on a flat surface of the sample. This course will provide an introduction to the theory of x-ray microanalysis by wavelength and energy dispersive spectrometry (WDS and EDS), ZAF matrix correction procedures and different imaging techniques including scanning backscattered electron (BE), scanning secondary electron (SE), scanning x-ray (by WDS or EDS, also known as compositional or elemental maps), and scanning cathodoluminescence (CL) imaging. Lab sessions will involve hands-on use of the JEOL JXA-733 Superprobe.

MI T Electron Microprobe Facility

Massachusetts Institute of Technology
Department of Earth, Atmospheric & Planetary Sciences

TABLE OF CONTENTS

	<u>Page number</u>
1. INTRODUCTION	3
2. ELECTRON SPECIMEN INTERACTIONS	3
2.1 ELASTIC SCATTERING	4
2.1.1 Electron backscattering	4
2.1.2 Interaction volume	5
2.2 INELASTIC SCATTERING	6
2.2.1 Secondary electron excitation	6
2.2.2 Bremsstrahlung or continuum x-ray generation	6
2.2.3 Characteristic x-ray generation	7
2.2.4 Interaction volume	9
3. MATRIX CORRECTIONS	12
3.1 Atomic number correction	13
3.2 Absorption correction	16
3.3 Characteristic fluorescence correction	19
3.4 Continuum fluorescence correction	20
3.5 $\phi(\rho z)$ corrections	20
4. DETECTORS IN ELECTRON MICROPROBES	22
4.1 ELECTRON DETECTORS	22
4.1.1 Everhart-Thornley detector	22
4.1.2 Solid-state diode detector	23
4.2 CATHODOLUMINESCENCE DETECTORS	25
4.3 X-RAY DETECTORS	26
4.3.1 Energy dispersive spectrometer	26
4.3.2 Wavelength dispersive spectrometer	26
5. COMPOSITIONAL IMAGING BY WDS	33
5.1 Defocusing correction during WDS compositional imaging	34
6. QUANTITATIVE ANALYSIS BY WDS	35
6.1 Background and peak overlap correction in WDS	37
6.2 Light element analysis by WDS	38
7. COMPARISON OF WDS AND EDS	42
8. REFERENCES	44
8.1 Sources and recommended reading	45
8.2 Acknowledgements	45
9. THE MIT ELECTRON MICROPROBE FACILITY	46
9.1 The electron microprobe at MIT	46
9.2 A short guide to dQant32 and dPict32	48

1. INTRODUCTION

X-rays are electromagnetic energies in the range of about 0.12-120 keV with wavelengths of 10 to 10^{-2} nanometers. In x-ray emission spectrometry, we utilize the x-ray portion of the electromagnetic spectrum emitted by the sample to measure concentration of elements by comparing with the emitted spectra from standards in which the concentration of the elements is known. Each element emits a set of characteristic x-rays at known energies. In electron microprobe analysis (also known as electron probe x-ray microanalysis, or EPMA), the typical range of x-ray energies analyzed are in the 0.12-10 keV range. Other regions of the electromagnetic spectrum are utilized to obtain concentrations by other techniques. For example, in spectrophotometry the visible light spectrum with wavelengths of 800-400 nm is analyzed. Identification of elements through x-rays was first suggested in 1913 by Moseley, who found that the frequency of emitted characteristic x-rays is a function of the atomic number of the emitting element.

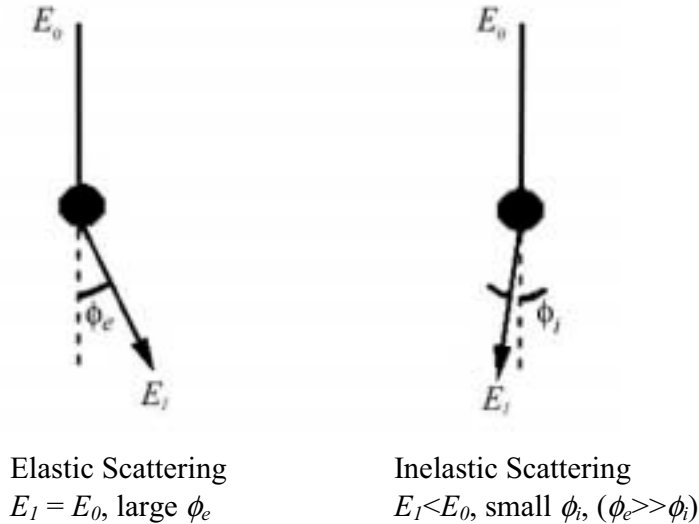
In the electron microprobe, x-rays are emitted by the sample in response to a finely focused electron beam incident on the sample at a right angle. Some of the beam electrons are scattered backward. The backscattered electrons, as well as the characteristic x-rays of the elements, carry information about the chemical composition of the sample. The idea to use a focused electron beam to excite x-rays in a small area for the purpose of x-ray spectrometry was first patented by Marton and Hillier in the 1940s, and the first electron microprobes were built in the early 1950s.

The electron microprobe serves two purposes: (a) it provides a complete quantitative chemical analysis of microscopic volumes of solid materials through x-ray emission spectral analysis; and (b) it provides high-resolution scanning electron, scanning x-ray (concentration maps) and scanning cathodoluminescence (CL) images. There are two types of scanning electron images: backscattered electron (BE) images, which show compositional contrast, and secondary electron (SE) images, which show enhanced surface and topographic features. Scanning cathodoluminescence images form by light emission in response to a scanning electron beam interacting with the sample. These images are very useful in studying trace element related compositional zoning in minerals like zircon.

Different types of inorganic solid materials can be analyzed by EPMA including metals and their alloys; synthetic compounds such as semiconductors and superconductors; and naturally occurring minerals such as oxides, silicates, sulfides and carbonates. Organic compounds such as polymers and biological specimens can also be studied, although special procedures and sample preparation techniques (such as freeze drying and cryo-sectioning) must be used. The spatial resolution (beam diameter) of the electron beam is about 1 μm . So, typically a volume of about 1 μm^3 is analyzed. Under favorable conditions, elemental concentrations as low as 10 ppm by weight (about 10^{-16} to 10^{-15} g) can be measured. Minimal sample preparation is required. A well polished surface is sufficient for analysis. Hence, the technique is considered nondestructive.

T2. ELECTRON SPECIMEN INTERACTIONS

When an electron beam strikes a target (that is, the sample), the electrons are scattered by the target atoms. There are two types of electron scattering:



where, E_0 is the energy of the incident electron; E_1 , the energy of the electron after scattering; ϕ_e , the elastic scattering angle; and ϕ_i , the inelastic scattering angle.

2.1 ELASTIC SCATTERING

Elastic scattering affects trajectories of beam electrons inside the specimen without significantly altering the kinetic energy of the electron (e.g., electron backscattering). The **cross-section, Q** (probability that a scattering event will occur), of elastic scattering for scattering angles greater than ϕ_e , is given by the screened Rutherford expression:

$$Q(>\phi_e) = 1.62 \times 10^{-20} (Z^2/E^2) \cot^2(\phi_e/2) \quad (2.1)$$

events.cm²/e⁻.atom; where, Z is the atomic number; and E , the incident electron energy (keV). Thus, the cross section of elastic scattering is proportional to the square of the atomic number of the target, and inversely proportional to the square of the incident energy of the electron beam.

2.1.1 Electron Backscattering

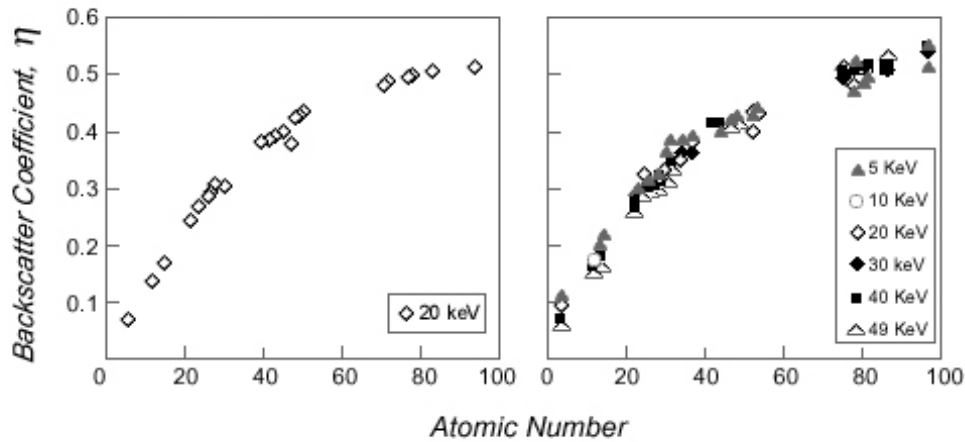
When the elastic scattering angle is greater than 90°, backscattering occurs. Even if the scattering angle is less than 90°, backscattering may occur through multiple scattering events at high angles. The **backscatter coefficient, η** , is defined as

$$\eta = n_{\text{BSE}}/n_{\text{B}} = i_{\text{BSE}}/i_{\text{B}} \quad (2.2)$$

where, n_B is the number of incident beam electrons and n_{BSE} is the number of backscattered electrons (i 's denote current). When the specimen is a homogeneous compound, η is given as:

$$\eta = \sum_j C_j \eta_j \quad (2.3)$$

where, j denotes each constituent element and C_j is the concentration of constituent element j . η increases monotonically with atomic number, although minor deviations occur between neighboring elements. It is not very sensitive to electron beam energies above 5 keV. It also increases monotonically with the tilt angle (angle between the beam and the perpendicular to the target surface) because of the dominant tendency of elastic scattering for forward scattering. As a result, η for all elements tend to converge at high tilt angles.



2.1.2 Interaction Volume

Monte Carlo electron-trajectory simulation provides a way to visualize the volume of the sample in which the beam electrons interact. In this simulation, equations for elastic and inelastic scattering are used to determine scattering angles, mean free-paths, and the rate of energy-loss of the electrons. From these parameters and equations of analytical geometry, an electron trajectory is simulated in a stepwise fashion from the location at which the electron enters the specimen to its final fate when it either leaves the specimen or loses all of its energy to be absorbed by the specimen.

Influence of beam energy: Experiments and Monte Carlo simulations of electron trajectories indicate that the size of the electron interaction volume in a specimen increases with the incident beam energy. There is less elastic scattering as beam energy increases (Eqn. 2.1) and the electrons are able to penetrate deeper into the specimen at higher beam energies. The depth of penetration, or range, is limited by the energy of the incident electrons.

Influence of atomic number: At a fixed incident beam energy, the interaction volume decreases with increasing atomic number because the cross-section of elastic scattering increases with the square of the atomic number (Eqn. 2.1). Experiments suggest that the interaction volume has a distinct pear shape for low atomic number targets, whereas, it becomes more and more spherical as the atomic number of the target increases.

Influence of specimen surface tilt: The interaction volume for a tilted specimen surface is smaller and asymmetric compared to the volume for a perpendicular incidence. Electrons tend to escape on one side of the interaction volume as the surface of the specimen is closer. Thus, the depth of penetration is also smaller.

Sampling depth of backscattered electrons: Most of the backscattered electrons come from the top part of the interaction volume. For example, Monte Carlo calculations suggest that 90% of the total backscattering is obtained in the top 17% of the total depth of electron penetration in Au and the top 29% of the total depth in C (at 0° tilt and 20 keV beam energy).

2.2 INELASTIC SCATTERING

Inelastic scattering involves transfer of energy from the beam electrons to the atoms of the specimen (e.g., generation of secondary electrons, Auger electrons, characteristic x-rays and bremsstrahlung or continuum x-rays). The trajectory of the beam electron is not altered significantly.

2.2.1 Secondary electron excitation

In metals, the conduction band electrons may be mobilized by inelastic scattering of the beam electrons. In semiconductors and insulators, inelastic scattering of beam electrons may lead to the promotion of loosely bound electrons from the valence band to the conduction band (electron-hole pair production), which may move through the specimen while serving as charge carriers. These specimen electrons are known as ***secondary electrons***. Some of these electrons may overcome the surface energy barrier and escape from the specimen. Secondary electrons are emitted at energies <50 eV and the majority (90%) of secondary electrons have energies <10 eV.

The ***secondary electron coefficient, δ*** , is defined as

$$\delta = n_{SE}/n_B = i_{SE}/i_B \quad (2.4)$$

where, n_B is the number of incident beam electrons and n_{SE} is the number of secondary electrons (i 's denote current). Compared to the backscatter coefficient, η , the secondary electron coefficient, δ , is relatively insensitive to the target atomic number. It generally increases as the electron beam energy decreases, and the tilt angle increases.

Although secondary electrons are generated throughout the interaction volume, the escape probability of these electrons from the surface of the sample drops sharply with depth. The *escape depth of secondary electrons is only about 1/100 of that for backscattered electrons* for incident beam energies in the range 10-30 keV. Thus, secondary electrons are useful in studying the physical characteristics of the surface of the sample. For secondary electron imaging, electrically nonconductive samples are usually coated with a thin layer of gold, which has a high secondary electron yield.

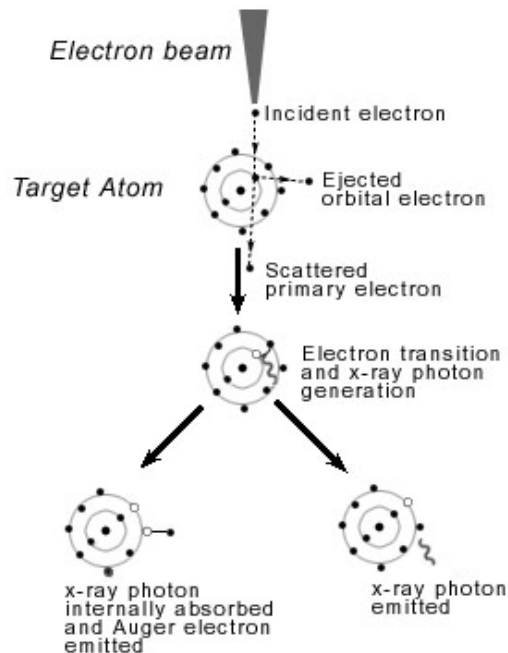
2.2.2 Bremsstrahlung or Continuum X-ray generation

An energetic beam electron may interact with the outer shells (such as the valence electrons) of the target atoms and undergo deceleration in the Coulombic field generated by

the outer shell electrons. The energy lost by the beam electron during this process is given off as a photon of electromagnetic energy, which may take on any value from a fraction to the total of the incident energy of the beam electron. The bremsstrahlung x-rays thus form a continuous spectrum from zero up to the beam energy. The maximum bremsstrahlung energy, known as the Duane-Hunt limit, provides a method to accurately measure the energy of the electron beam.

2.2.3 Characteristic X-ray generation by ionization of inner shells

A tightly bound inner shell electron may be ejected from a specimen atom as a result of inelastic scattering of a beam electron, if its energy is higher than the **critical excitation energy**, E_c (also known as **x-ray absorption edge energy**), of the target atom for the inner shell under consideration. The energy of the beam electron is diminished by an amount equal to E_c and subsequent decay of the target atom from its excited state, which involves the transfer of an electron from an outer shell to the inner shell, results in the generation of a characteristic x-ray photon. This photon may be emitted from the atom, or it may be internally absorbed while ejecting another outer shell electron (an Auger electron). The fraction of x-rays emitted (**characteristic x-ray** or **fluorescent yield**, ω) for a specific shell increases with the atomic number, whereas the **Auger yield**, α , decreases.



Characteristic energy lines are named as follows:

$K\alpha$: when vacancy in K-shell is filled by a transition from L-shell,

$K\beta$: when vacancy in K-shell is filled by a transition from M-shell,

$L\alpha$: when vacancy in L-shell is filled by a transition from M-shell,

$L\beta$: when vacancy in L-shell is filled by a transition from N-shell,

$M\alpha$: when vacancy in M-shell is filled by a transition from N-shell, etc.

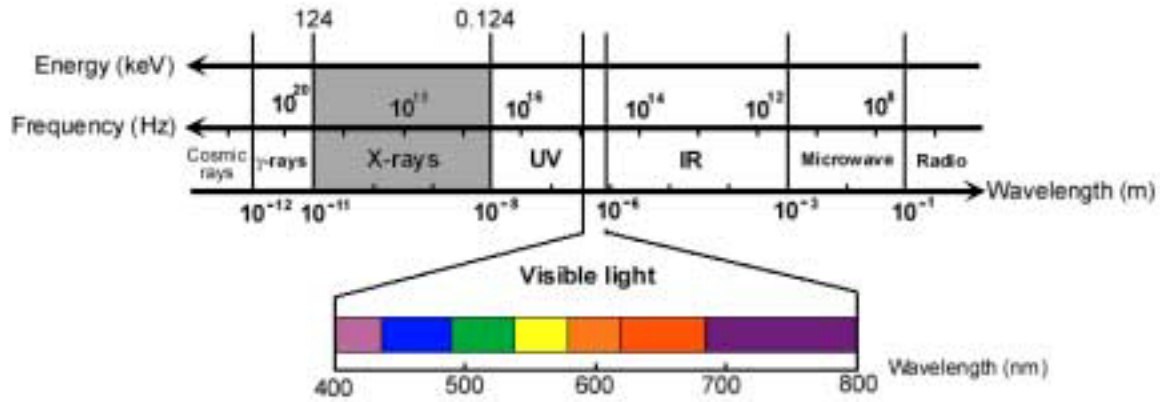
The **energy** of an x-ray photon is given by

$$E = h\nu \quad (2.5)$$

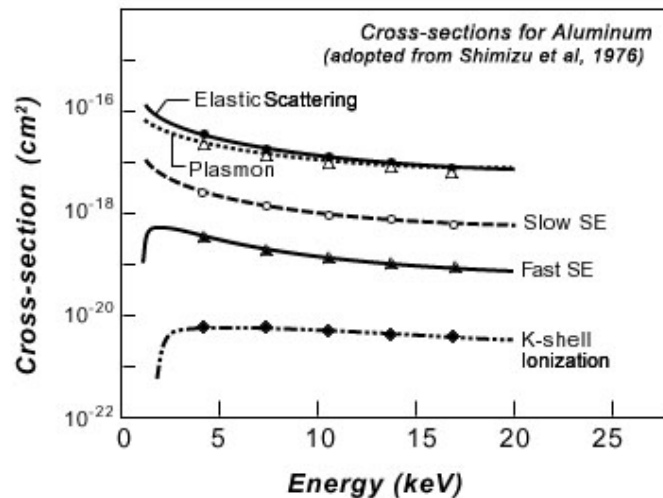
Where, h is the Planck's constant (6.626×10^{-34} Joule.sec = $6.626 \times 10^{-34} / 1.6021 \times 10^{-16}$ keV.sec) and the frequency $\nu = c/\lambda$, c being the speed of light in vacuum (2.99793×10^{18} Å/sec) and λ being the **wavelength**. Thus, the wavelength is related to the energy as follows:

$$\lambda = hc/E = 12.398/E \quad (2.6)$$

where, λ is in Å and E is in keV.



Cross-sections of all types of inelastic scattering decrease with increasing incident energy. This is illustrated for aluminum as follows:



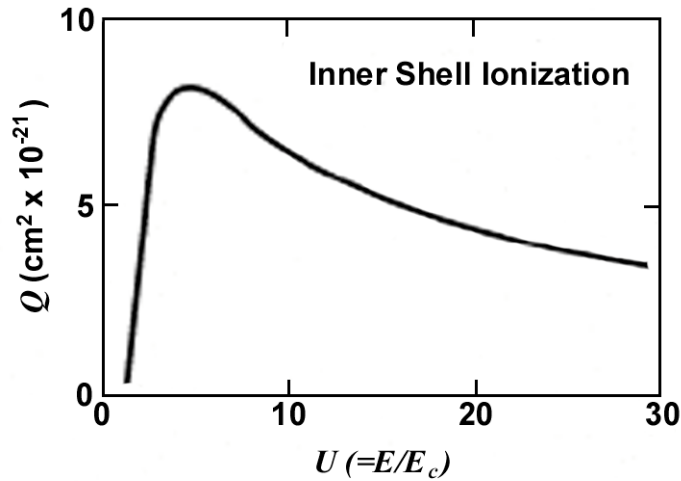
For **inner shell ionization**, the cross-section is given by Bethe as follows:

$$Q = 6.51 \times 10^{-20} [(n_s b_s) / (UE_c^2)] \ln(c_s U) \quad (2.7)$$

ionizations. $\text{cm}^2/e^- \cdot \text{atom}$), where n_s is the number of electrons in a shell or subshell (e.g., $n_s=2$ for a K shell), b_s and c_s are constants for a particular shell, E_c (keV) is the critical excitation energy of the shell, and U is the **overvoltage**, E/E_c , where E (keV) is the instantaneous beam energy. For the K-shell, the recommended values of the constants are $b_s=0.3$ and $c_s=1$ at low overvoltages, and $b_s=0.9$ and $c_s=0.65$ at higher voltages ($4 < U < 25$).

Continuous energy loss approximation: For all inelastic scatterings, Bethe gave the following equation:

$$dE/ds = -7.85 \times 10^4 (Z\rho/AE_m) \ln(1.166E_m/J) \quad (2.8)$$



where, the constant is equal to $2\pi e^4 N_0$; e being the electronic charge and N_0 , the Avogadro's number; Z is the atomic number; A (g/mole), the atomic weight, ρ (g/cm^3), the density, E_m (keV), the average energy along path segment s , and J , the mean ionization potential given by Berger & Seltzer:

$$J \text{ (keV)} = (9.76Z + 58.82 Z^{0.19}) \times 10^{-3} \quad (2.9)$$

Joy & Luo further modified the Bethe expression for low beam energies ($E < 7J$), by substituting J^* for J , where

$$J^* = J / (1 + kJ/E) \quad (2.10)$$

where, $k = 0.731 + 0.0688 \log Z \quad (2.11)$

2.2.4 Interaction volume

Electron range: The electron range is the distance traveled by the beam electrons until they lose all their energy. The total distance traveled by an electron undergoing inelastic scattering (Bethe range) may be given as,

$$R = \int_{E=E_0}^{E=0} \frac{1}{dE/ds} dE \quad (2.12)$$

where, dE/ds may be substituted from Eqn. 2.8. This overestimates the electron range because it neglects the effect of elastic scattering. The Kanaya-Okayama range for the combined effects of elastic and inelastic scattering is as follows:

$$R_{KO} = KE_0^n/\rho \quad (2.13)$$

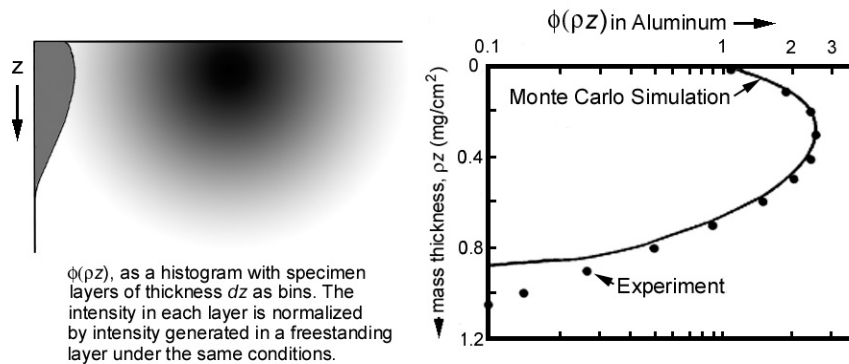
(μm), where, $K = 0.0276A/Z^{0.889}$, A (g/mole), the atomic weight, Z , the atomic number, ρ (g/cm^3), the density, E_0 (keV), the incident beam energy, and $n = 1.67$.

X-ray range: Characteristic x-rays can be produced only when the incident energy exceeds E_c , the critical excitation energy. Thus, the x-ray range is always smaller than the electron range. The x-ray range according to Anderson & Hassler is:

$$R = K(E_0^n - E_c^n)/\rho \quad (2.14)$$

(μm) where, $K = 0.064$, and $n = 1.68$. The range of primary x-ray generation for a given x-ray line is the critical parameter in estimating the sampling volume for x-ray microanalysis.

Depth-distribution function, $\phi(\rho z)$: The $\phi(\rho z)$ function for x-ray production can be thought of as a histogram giving the relative number of x-rays generated in a slice of the specimen of thickness dz . The histogram is normalized by the number of x-rays the beam would produce in a freestanding layer of thickness equal to dz and of the same composition. The upper part (layers) of the interaction volume always produces more x-rays than a freestanding layer because as the incident electrons are scattered and backscattered, they travel obliquely or backward in the layer of thickness dz interacting with more of the specimen atoms. As the depth increases, however, the electrons lose their energy and their ability to produce inner-shell ionizations and x-ray generation ceases when the overvoltage U drops below unity.



From definition, the total x-ray intensity generated by element i is

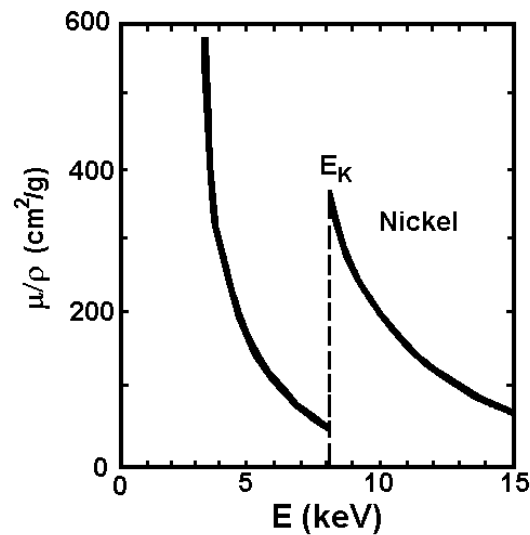
$$I_{gen} = \phi(\Delta\rho z) \int_0^{\infty} \phi(\rho z) d(\rho z) \quad (2.15)$$

where, $\phi(\Delta\rho z)$ is the intensity generated in a freestanding layer of thickness $\Delta\rho z$ and of the same composition.

X-ray absorption: The generated x-rays may undergo photoelectric absorption upon transferring part or all of its energy to an electron of a another specimen atom, which may eject the electron and go in an excited atomic state. The final emitted intensity of an x-ray is given by:

$$I = I_0 \exp^{-(\mu/\rho)(\rho t)} \quad (2.16)$$

where, I_0 is the initial generated intensity, ρ is the density, t is the thickness of the specimen slab and (μ/ρ) is the **mass absorption coefficient** (cm^2/g) of the specimen. Absorption is maximum when the energy of the x-ray photon is slightly above the critical excitation energy of the shell concerned.



Plot of the mass absorption coefficient as a function of x-ray energy in Nickel

The mass absorption coefficient of the specimen decreases with increasing incident x-ray photon energy, until the incident energy is slightly higher than an absorption edge (or critical excitation energy) of an element present in the specimen, where (μ/ρ) of the specimen jumps to a high value.

Element (Atomic No.)	$E_{K\alpha}$ (keV)	$E_{K\beta}$ (keV)	$E_{c(K)}$ (keV)	$(\mu/\rho)^{\text{NiK}\alpha}_{\text{elem.}}$ (cm^2/g)
Mn(25)	5.895	6.492	<u>6.537</u>	<u>344</u>
Fe(26)	6.4	7.059	<u>7.111</u>	<u>380</u>
Co(27)	6.925	7.649	7.709	53
Ni(28)	<u>7.472</u>	8.265	8.331	59
Cu(29)	8.041	8.907	8.98	65.5

The data in the above table indicates that $\text{NiK}\alpha$, with an energy of 7.472 keV, will be efficiently absorbed in Fe and Mn, whose critical excitation energies are 7.111 keV and 6.537 keV respectively.

X-ray fluorescence: X-ray fluorescence may occur as a consequence of photoelectric absorption of x-rays. As the excited specimen atom (excited by absorption of incident primary x-ray) relaxes, it generates characteristic x-rays known as secondary x-rays. Secondary radiation may be induced by either incident characteristic or continuum x-rays. Since x-rays have a much greater range in matter than electrons, the *range of x-ray induced fluorescence is also much greater (~10 times) than the primary electron range*. The volume may be as much as 1000 times greater than the primary interaction volume.

The above table also demonstrates that NiK α (and K β) can only be fluoresced by CuK β as the Ni absorption edge is at 8.331 keV, and only CuK β has an energy greater than that (8.907 keV). CuK β will be absorbed in the process. The other elements in the alloy will be fluoresced as follows (both K α and K β of the element may be fluoresced):

Element	Radiation causing fluorescence
Mn	FeK β , CoK α , CoK β , NiK α , NiK β , CuK α , CuK β
Fe	CoK β , NiK α , NiK β , CuK α , CuK β
Co	NiK β , CuK α , CuK β
Ni	CuK β
Cu	none

3. MATRIX CORRECTIONS

Castaing, in 1951, noted that the *primary generated* x-ray intensities are roughly proportional to the respective mass-fractions of the emitting element. Thus,

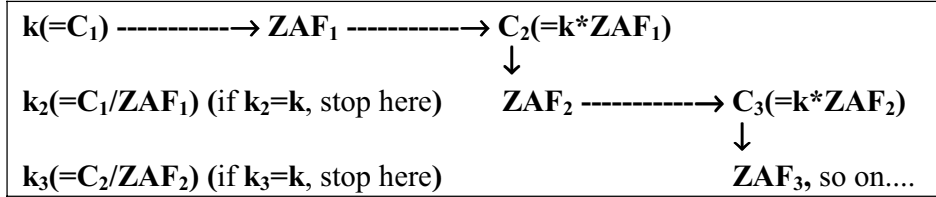
$$C_i/C_{(i)} = I_i/I_{(i)} = k_i \quad (3.1)$$

where, C_i and $C_{(i)}$ are the weight concentration of element i in the unknown and the standard, respectively; and I_i and $I_{(i)}$ are the primary generated x-ray intensities in the unknown and standard, respectively and k_i is a constant for element i known as the ***k-ratio***. However, the primary generated x-rays may be absorbed or it may generate secondary x-rays by fluorescence in the specimen. Further, some of the primary electrons may be backscattered out of the specimen and consequently, the number of inner-shell ionizations will be less than expected. Hence, corrections must be applied to the measured x-ray intensities. The atomic number correction, **Z** (related to electron backscattering), the absorption correction, **A**, and the fluorescence correction, **F** are the three constituents of the ***matrix correction***. The above equation is modified for *measured* x-ray intensities as:

$$C_i/C_{(i)} = [\mathbf{ZAF}]_i I_i/I_{(i)} = [\mathbf{ZAF}]_i k_i \quad (3.2)$$

Z, **A** and **F** of an element are matrix effects and depend on the concentration of other elements present in the matrix (interaction volume). Since the concentrations are not known in a specimen before the analysis, the ZAF factors are also unknown. Thus, an iterative approach is adopted. The measured k-ratios (k_i) are used as a first estimate of the concentration of the elements and the ZAF factors are calculated. The concentrations (C_i) are then calculated by multiplying the k-ratios with the corresponding ZAF factors calculated in

the last step. The ZAF factors are then recalculated using the C_i values obtained in the last step. The k-ratios are now recalculated ($k_i = C_i/[ZAF]_i$) and compared to the original k-ratios. The process is repeated until the calculated k-ratios are the same as the original k-ratios. The concentrations are calculated by multiplying the original k-ratios with the final set of ZAF factors. The process is demonstrated in the following flow-chart:



3.1 Atomic number correction (Z)

The atomic number effect arises from two phenomena: electron backscattering (R) and electron retardation or stopping power (S), both of which depend on the average atomic number of the target. Therefore, if there is a difference between the average atomic number of the specimen, and that of the standard, an atomic number correction is required. R and S are defined as:

R : ratio of number of x-ray photons actually generated, to number of x-ray photons generated if there were no backscatter;

S : $-(1/\rho)(dE/ds)$, where ρ is the density and dE/ds , rate of energy loss (Eqn. 2.8).

The atomic number correction Z_i for element i is given by Duncumb & Reed as:

$$Z_i = \frac{R_i \int_{E_c}^{E_0} \frac{Q}{S} dE}{R_i^* \int_{E_c}^{E_0} \frac{Q}{S^*} dE} \quad (3.3)$$

where, Q is the ionization cross-section (Eqn. 2.7), and R and S marked by * are for the specimen (unmarked R and S are for the standard). The backscattering factor, R_i , varies both with the atomic number and the overvoltage ($U=E_0/E_c$). As the overvoltage decreases toward unity, fewer electrons with energies greater than E_c are backscattered and hence, there is less of a loss of ionization. R_i is given as:

$$R_i = \sum_j C_j R_{ij} \quad (3.4)$$

where, j represents each of the elements present in the standard or the specimen. Yakowitz et al. give R_{ij} as:

$$R_{ij} = R'_1 - R'_2 \ln(R'_3 Z_j + 25) \quad (3.5)$$

where,

$$R'_1 = 8.73 \times 10^{-3} U^3 - 0.1669 U^2 + 0.9662 U + 0.4523 \quad (3.6)$$

$$R'_2 = 2.703 \times 10^{-3} U^3 - 5.182 \times 10^{-2} U^2 + 0.302 U - 0.1836 \quad (3.7)$$

$$R'_3 = (0.887 U^3 - 3.44 U^2 + 9.33 U - 6.43)/U^3 \quad (3.8)$$

S is related to the continuous energy loss expression (Eqn. 2.8). S_i is given as:

$$S_i = \sum_j C_j S_{ij} \quad (3.9)$$

where, j represents each of the elements present in the standard or the specimen. Thomas approximates the mean energy E_m (Eqn. 2.8) as $(E_0 + E_c)/2$. Thus, S_{ij} may be given as:

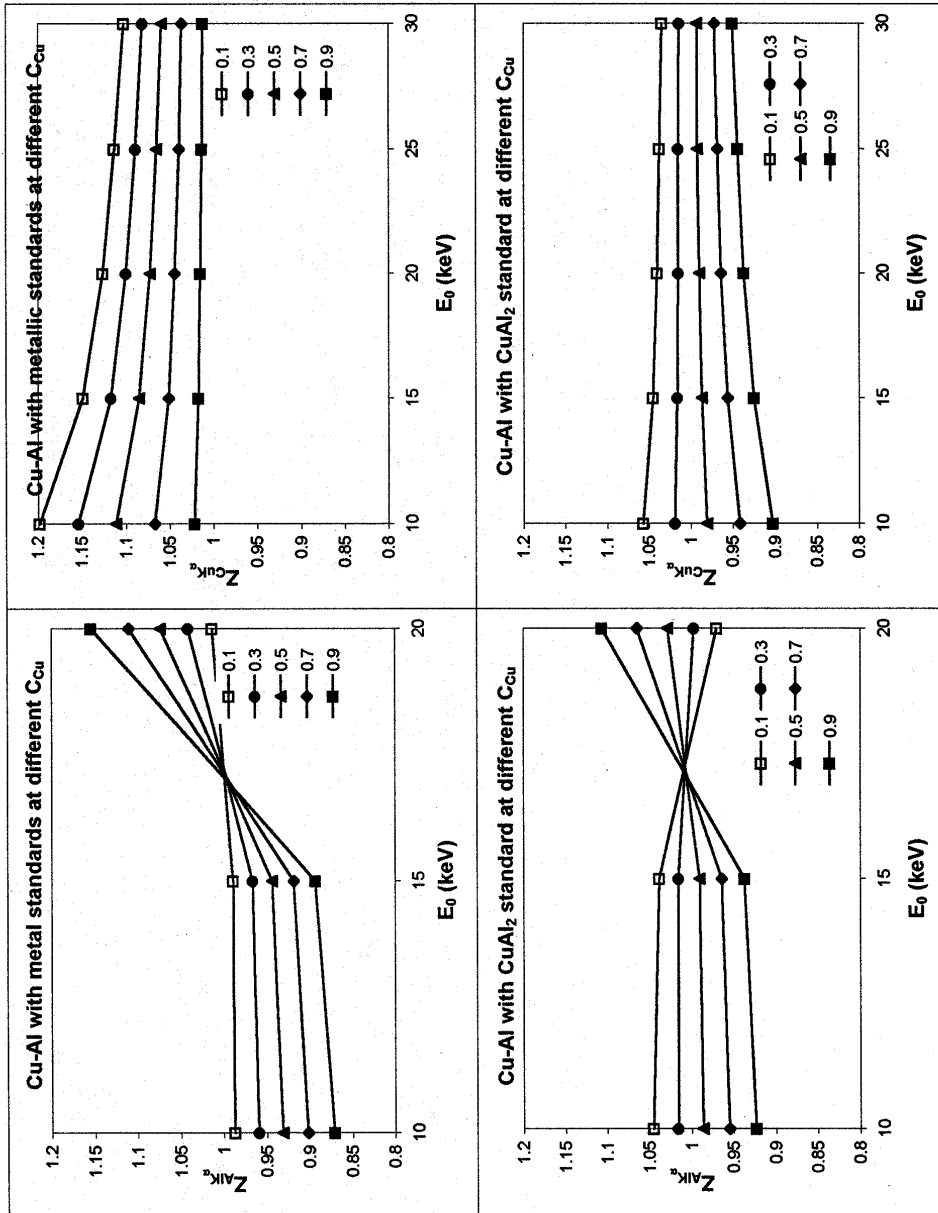
$$S_{ij} = (\text{const}) [(2Z_j/A_j)/(E_0 + E_c)] \ln[583(E_0 + E_c)/J_j] \quad (3.10)$$

A simplifying assumption is often made that Q is a constant and cancels out in the expression for Z_i . The same happens to the constant term in Eqn. 2.8. Further, avoiding the integration in Eqn. 3.3, Z_i can be approximately given as:

$$Z_i = (R_i S_i^*) / (R_i^* S_i) \quad (3.11)$$

To demonstrate the effect of the difference in average atomic number of the specimen and the target on the atomic number correction, the correction is calculated using the above equations (Duncumb & Reed, 1968; Yakowitz et al., 1973; Thomas, 1964; Berger & Seltzer, 1964) for a complete range of Cu-Al alloys with respect to metal standards ($Z_{Al}=13$, $Z_{Cu}=29$) as well as a θ -phase (CuAl₂; avg. atomic no., $Z=21.6$) standard. Let us consider the 90wt% Al-10wt% Cu composition ($Z=14.6$). Since there is a large atomic number difference between the specimen and the Cu standard, the atomic number correction for CuK α is also large ($Z_{CuK\alpha} = 1.149$ at $E_0=15$ keV), compared to the correction for AlK α ($Z_{AlK\alpha} = 0.989$) where the atomic number difference is small. When the θ -phase is used as a standard, the atomic number difference with respect to CuK α decreases, whereas it increases with respect to AlK α . As a result, $Z_{CuK\alpha}$ decreases to 1.045 (a decrease of ~60% in the correction) and $Z_{AlK\alpha}$ increases to 1.038 under the same condition of $E_0=15$ keV. An important conclusion from these plots is that it is always preferable to choose a standard whose composition is similar to the specimen.

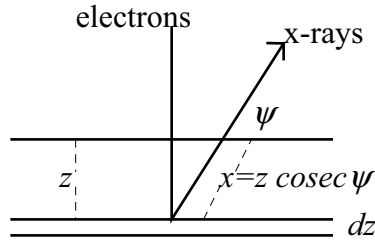
It should be noted in the graphs for AlK α that the crossover at ~17 keV of the $Z_{AlK\alpha}$ values may be an artifact of the complex polynomial fit of the Duncumb & Reed data by Yakowitz et al. Yakowitz's equations probably do not work above a certain value of U , $U_{Al}=9.62$ (corresponding to $E_0=15$ keV) in this case. The relation between Z_i and U is complex, although in general, Z_i decreases very slowly with an increase in U . The uncertainty in Z_i does not change much as U increases. Since, as we will see later, high U values require large absorption corrections, a low U is preferable.



3.2 Absorption correction (A)

Intensity of an emitted x-ray photon for element i from depth z , along an angle ψ (angle measured from the sample surface, or the take-off angle) for normal incidence of an electron beam is given by (following Eqn. 2.16):

$$I'_{i(em)} = I'_{i(0)} \exp^{-(\mu/\rho)^i (\rho z \operatorname{cosec} \psi)} \quad (3.12)$$



Consequently, the x-ray intensity emitted from an infinitesimal layer $d(\rho z)$ at a depth z is given by,

$$dI'_i = \phi_i(\rho z) \exp^{-(\mu/\rho)^i (\rho z \operatorname{cosec} \psi)} d(\rho z) \quad (3.13)$$

where, $\phi_i(\rho z)d(\rho z)$ is the intensity of x-ray generated in the layer $d(\rho z)$. The total intensity emitted thus becomes,

$$I'_{i(em)} = \phi_i(\Delta \rho z) \int_0^\infty \phi_i(\rho z) \exp^{-(\mu/\rho)^i (\rho z \operatorname{cosec} \psi)} d(\rho z) \quad (3.14)$$

The total generated x-ray intensity is given by Eqn. 2.15. Thus, the *absorption function*, $f(\chi_i)$, defined as $I_{i(em)}/I_{i(gen)}$, is given by,

$$f(\chi_i) = \frac{\int_0^\infty \phi_i(\rho z) \exp^{-\chi_i \rho z} d(\rho z)}{\int_0^\infty \phi_i(\rho z) d(\rho z)} \quad (3.15)$$

where,

$$\chi_i = (\mu/\rho)^i \operatorname{cosec} \psi \quad (3.16)$$

The absorption correction A_i for an element i in a compound is given by:

$$A_i = f(\chi_i)/f(\chi_i)^* \quad (3.17)$$

where, the specimen is noted by *. The $\phi(\rho z)$ function is related to the x-ray energies, the voltage and some other physical parameters through equations. It can be measured through experiments or described by empirical or semi-empirical relations. According to Philibert, $f(\chi_i)$ can be given by the following semi-empirical relation:

$$f(\chi_i) = \left[\left(1 + \frac{\chi_i}{\sigma_i} \right) \left(1 + \frac{\chi_i}{\sigma_i} \frac{h_i}{1+h_i} \right) \right]^{-1} \quad (3.18)$$

where,
$$h_i = 1.2A_i/Z_i^2 \quad (3.19)$$

$$\sigma_i = 4.5 \times 10^5 / (E_0^{1.65} - E_{i(c)}^{1.65}) \quad (3.20)$$

σ , which takes into account the accelerating voltage and the critical excitation energy, is known as the Lenard coefficient and its formulation is based on Duncumb & Shields and Heinrich. For multielement compounds, the average value of h , and (μ/ρ) of specimen for radiation from element i are evaluated as follows:

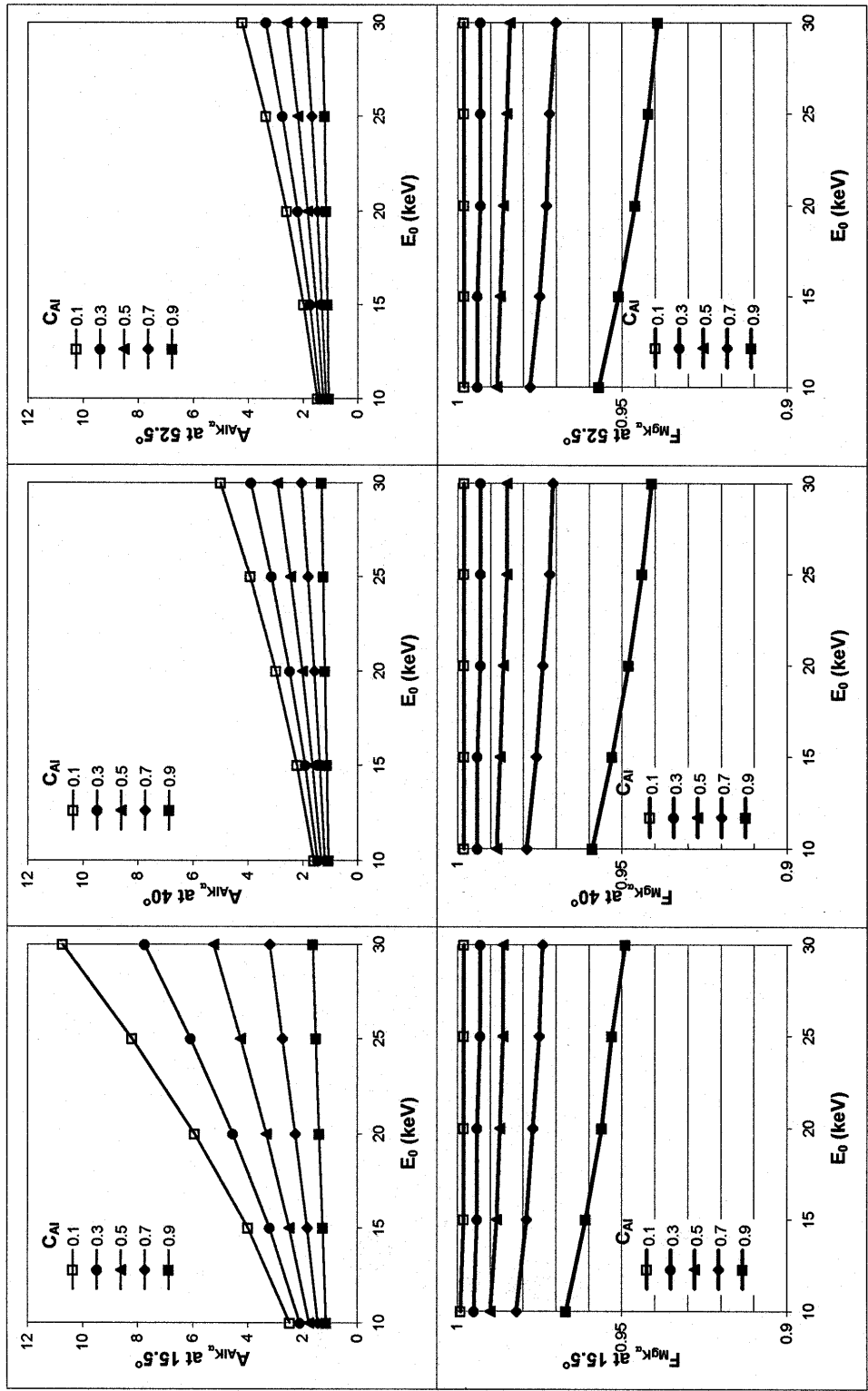
$$h_i = \sum_j h_j C_j \quad (3.21)$$

$$(\mu/\rho)_{spec}^i = \sum_j (\mu/\rho)_j^i C_j \quad (3.22)$$

Philibert obtained his equation by fitting the form of experimental $\phi(\rho z)$ curves available at that time. He made a simplification by setting $\phi_0=0$ (the value of $\phi(\rho z)$ at the surface). However, ϕ_0 is always >1 due to the effect of backscattered electrons. Hence, in cases where most of the x-rays are generated close to the surface (for example, light element (C,N,O) x-rays in a metal matrix (Ti,Fe,Cu)), the Philibert equation will produce erroneous results.

The absorption correction is a function of the mass absorption coefficients, the take-off angle and the accelerating voltage. To understand the effect of these three parameters on the absorption correction, the Mg-Al binary alloy is considered. $AlK\alpha$ ($E_K=1.487$ keV) is highly absorbed in Mg ($E_c=1.303$ keV) with $(\mu/\rho)_{Mg}^{AlK\alpha}=4168$ cm²/g (Heinrich, 1986). The following plots show calculated absorption corrections for $AlK\alpha$ (using the equations of Philibert, 1963; Duncumb & Shields, 1966; and Heinrich, 1969; and the E_c and (μ/ρ) tabulations of Bearden, 1964 and Heinrich, 1986 respectively) for different compositions of the Mg-Al alloy under different E_0 and ψ conditions. Three key conclusions emerge from these plots: the absorption correction, $A_{AlK\alpha}$, increases with increasing operating voltage, decreasing take-off angle and increasing Mg in the specimen.

Minimizing the path-length of the x-ray generated within the sample will minimize its absorption. Thus, it is not surprising that lower operating voltages and higher take-off angles lead to a lower absorption correction. Further, more Mg in the sample leads to a more efficient absorption of the $AlK\alpha$. Any error in the mass absorption coefficient propagates into the final result. The effect of uncertainties in mass absorption coefficients is low when the value of the absorption function $f(\chi)$ is greater than 0.7. Most electron microprobes have fixed take-off angles. Thus, the operator should choose a low overvoltage to minimize the absorption correction.



3.3 Characteristic fluorescence correction (F)

Fluorescence correction is applied only when the critical excitation energy of the the element is lower than any of the x-rays generated by other elements in the specimen. The fluorescence correction for element i in a compound of j elements is given by:

$$\mathbf{F}_i = \frac{\left(1 + \sum_j \left\{ I_{ij}^f / I_i \right\}\right)}{\left(1 + \sum_j \left\{ I_{ij}^f / I_i \right\}\right)^*} \quad (3.23)$$

where, I_{ij}^f is the intensity of radiation of element i produced by fluorescence by element j , and I_i is the intensity of electron-generated radiation of element i . For a pure element standard, the numerator reduces to unity. The ratio I_{ij}^f/I_i is given by Castaing and modified by Reed as:

$$I_{ij}^f / I_i = C_j Y_0 Y_1 Y_2 Y_3 P_{ij} \quad (3.24)$$

where, $Y_0 = 0.5[(r_i-1)/r_i][\omega_j A_i/A_j]$ (3.25)

where, r_i is the absorption edge jump-ratio; $(r_i-1)/r_i$ is 0.88 for K-line, 0.75 for L-line; and ω_j is the fluorescent yield,

$$Y_1 = [(U_j-1)/(U_i-1)]^{1.67} \quad (3.26)$$

$$Y_2 = (\mu/\rho)_i^j / (\mu/\rho)_{spec}^j \quad (3.27)$$

where, $(\mu/\rho)_i^j$ is the mass absorption coefficient of element i for radiation from element j ; and $(\mu/\rho)_{spec}^j$ is the mass absorption coefficient of the specimen for radiation from element j ,

$$Y_3 = [\ln(1+u)]/u + [\ln(1+v)]/v \quad (3.28)$$

where, $u = [(\mu/\rho)_{spec}^i / (\mu/\rho)_{spec}^j] \operatorname{cosec} \psi$ (3.29)

and $v = 3.3 \times 10^5 / [(E_0^{1.65} - E_c^{1.65}) (\mu/\rho)_{spec}^j]$ (3.30)

and, P_{ij} is a factor for the type of fluorescence occurring (e.g., for K line fluorescing K line $P_{ij}=1$; for K-L, 4.76; for L-K, 0.24).

The fluorescence correction thus depends on absorption edge jump-ratio (r), the fluorescent yield (ω) of the fluorescer element, mass absorption coefficients, the take-off angle and the operating voltage. To understand the effect of ψ and E_0 on the fluorescence correction, the Mg-Al binary alloy is again considered. Since AlK α is highly absorbed in Mg and it has a higher energy than the K-shell critical excitation of energy of Mg, it is expected that MgK α will be fluoresced. Using the above equations (Castaing, 1951 and Reed, 1965), ω from Bambynek et al. (1972), (μ/ρ) from Heinrich (1986) and E_c from Bearden (1964), $\mathbf{F}_{\text{MgK}\alpha}$ in a range of Mg-Al compositions are calculated under different ψ and E_0 conditions.

The plots show that $F_{MgK\alpha}$ increases with increasing E_0 , increasing ψ and increasing Al in the specimen. However, a high ψ is required to minimize the absorption correction which is more significant in most cases. It has been noted that although the fluorescence correction is low at low ψ , the error associated with it does not increase at high ψ angles. Thus, a low E_0 and high ψ angle is recommended.

3.4 Continuum fluorescence correction

The continuum x-rays always contain quanta of energy sufficient to excite any characteristic radiation that can be directly excited by the beam electrons, since there is always some continuum radiation in the range E_c to E_0 . Hence, in correcting for continuum induced fluorescence, the effect must be integrated over an energy range E_c to E_0 . Myklebust et al. (1979) came to the conclusion that fluorescence induced by Brehmstrahlung radiation may be ignored if $f(\chi)$ is less than 0.95, C_i (concentration of the element) is more than 0.5 and Z_{std} (average atomic number) is close to Z_{spec} . Choice of low overvoltage and high take-off angle are usually enough to avoid continuum fluorescence correction. However, when a heavy component is surrounded by a light matrix (e.g., U in a common silicate mineral), $f(\chi)$ may be greater than 0.95 and continuum fluorescence may be significant. In this case, the lowest energy characteristic x-ray line of the element being analyzed should be chosen.

3.5 The $\phi(\rho z)$ correction procedure

The $\phi(\rho z)$ method uses calculated or measured $\phi(\rho z)$ curves to determine the atomic number and absorption corrections. The $\phi(\rho z)$ curves are fitted through empirical or semi-empirical equations. The $\phi(\rho z)$ method effectively deals with the corrections for atomic number and absorption in a single equation. The atomic number correction for element i is obtained by calculating the area under the $\phi(\rho z)$ curve for the standard and divide it by the area under the $\phi(\rho z)$ curve for the specimen. Following Eqn. 16, we can write:

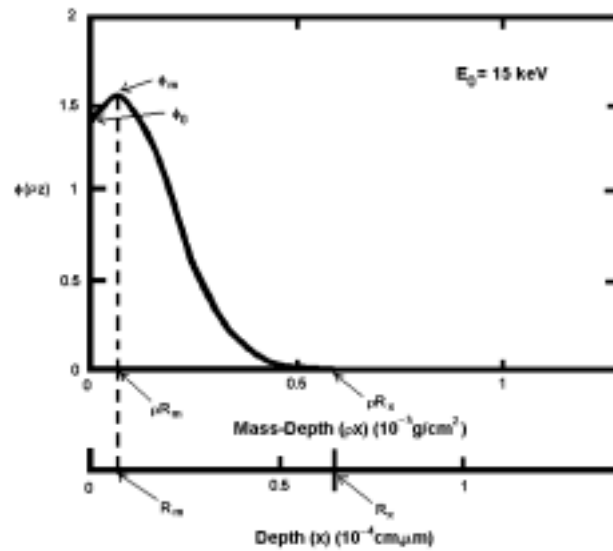
$$Z_i = \frac{\int_0^\infty \phi_i(\rho z) d(\rho z)}{\int_0^\infty \phi_i^*(\rho z) d(\rho z)} \quad (3.31)$$

Combining this with the absorption correction (Eqn. 3.15 and 3.16), we obtain:

$$Z_i A_i = \frac{\int_0^\infty \phi_i(\rho z) \exp^{-\chi_i \rho z} d(\rho z)}{\int_0^\infty \phi_i^*(\rho z) \exp^{-\chi_i \rho z} d(\rho z)} \quad (3.32)$$

In the above equation, $\phi(\rho z)$ is modeled empirically in terms of four parameters α , β , γ and $\phi(0)$ (Packwood and Brown, 1981), or semi-empirically in terms of three parameters $\phi(0)$, R_m and R_x and the integral of the $\phi(\rho z)$ distribution (Pouchou and Pichoir, 1984); where, $\phi(0)$ is the value of $\phi(\rho z)$ at $\rho z=0$, R_m is the depth at which the value of $\phi(\rho z)$ is maximum and R_x is the maximum depth of x-ray production.

Eqn. 3.32 is finally combined with the fluorescence correction (Eqn. 3.23) to obtain the full ZAF correction. The ZAF and the $\phi(\rho z)$ correction schemes are thus closely related.



Schematic for the measurement of $\phi(\rho z)$ curve.

One way to experimentally measure $\phi(\rho z)$ curves is known as the tracer technique (Castaing, 1951). To measure $\phi(\rho z)$ for $\text{CuK}\alpha$, a thin film of Zn, $\Delta(\rho z)$ in mass-thickness (the tracer), is deposited on a substrate and coated by a number of successive layers of Cu, each $\Delta(\rho z)$ in mass-thickness (matrix). The emitted intensity of $\text{ZnK}\alpha$ from the tracer is measured by placing the beam on each successive Cu-layer above the tracer. The intensity from the thin-film Zn tracer serves as the isolated thin film in space. The $\phi(\rho z)$ curve can be calculated after correction for the absorption of $\text{ZnK}\alpha$ from the tracer in the overlying matrix layers.

Zn is selected as the tracer in this case because it is of similar atomic number to Cu and the $\text{ZnK}\alpha$ x-ray line has an energy similar to but higher than that of $\text{CuK}\alpha$, so that it is not fluoresced by $\text{CuK}\alpha$.

4. DETECTORS IN ELECTRON MICROPROBES

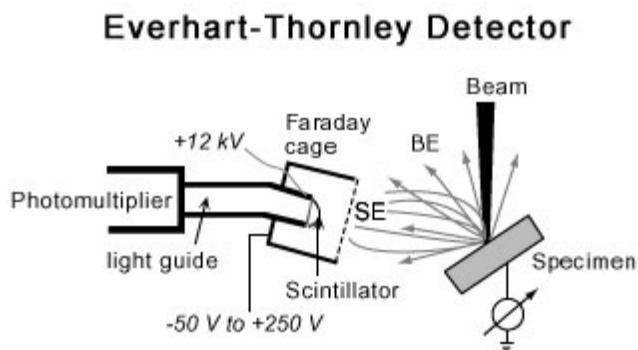
The electron microprobe can be used to obtain high resolution images of the surface of a specimen by rastering the electron beam over an area of the surface. These are called scanning images. A scanning image can be obtained from the electron signal, as in a secondary electron (SE) image or a backscattered electron (BE) image, or it can be from the x-ray signal, as in elemental x-ray images. X-ray images may be obtained either through the wavelength dispersive spectrometers or the energy dispersive spectrometer. A third kind of image is obtained from the light signal and is called a scanning cathodoluminescence (CL) image. In this section we will consider detectors commonly found on scanning electron microscopes and electron microprobes.

4.1 ELECTRON DETECTORS

Because of the energy differences between backscattered and secondary electrons, different detector setups are required for the detection of the two types of electron signal. Backscattered electrons are a result of multiple elastic scattering and have energies between 0 and E_0 (the beam energy). Secondary electrons, which are specimen electrons mobilized by the beam through inelastic scattering, have energies in the range 0-50 eV with a most probable energy of 3-5 eV.

4.1.1 Everhart-Thornley (E-T) detector for topographic contrast

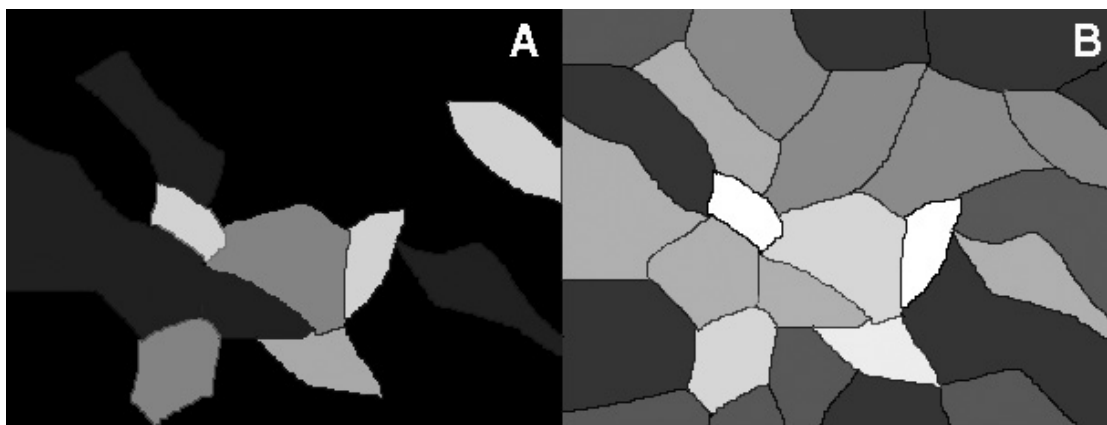
The E-T detector consists of a scintillator, which may be a doped plastic or glass or a CaF_2 crystal doped with Eu, and serves as the primary target for the electrons. Photons produced in the scintillator, which is kept at a large positive potential of 10 to 12 kV to attract the incoming electrons, travels through a light guide, a solid plastic or glass rod, to a photomultiplier with a high gain. The photons are converted back to electrons in the photomultiplier and the current is amplified by an attached amplifier. The signal is



synchronously displayed on an oscilloscope CRT as the beam scans over an area of the sample thus forming a scanning electron image.

The scintillator is surrounded by a Faraday cage which is insulated from the scintillator bias. By applying a selectable negative or positive potential (-50 to +250 V) to the Faraday cage, one can regulate the type of electrons (backscattered or secondary) to be detected by the scintillator. When the E-T detector is negatively biased, only the high energy backscattered electrons are detected, and the low energy secondary electrons are repelled away. A positively biased E-T detector accepts both backscattered and secondary electrons. Secondary electrons traveling in a direction away from the detector are actually attracted toward it because of the positive potential. A large component of the signal is, however, indirectly generated secondary electrons from the chamber walls excited by stray backscattered electrons. These secondary electrons actually contain information about the specimen (not the walls) as they represent a remote backscatter signal originated at the specimen.

The E-T detector is an invaluable tool for topographic imaging. Topographic contrast is achieved by this detector in the following way. Since the E-T detector is located on one side of the specimen, it has a small solid angle of collection and it is at a low take-off angle relative to the horizontal plane. Hence, it receives a highly directional view of the specimen. As a result, when imaging a fractured surface, the faces directly in the line-of-sight of the detector appear much brighter than other faces. If the detector is negatively biased, secondary electrons are completely rejected and the other faces appear dark producing a topographic shadowing effect. This harsh contrast is reduced when the detector is positively biased because secondary electrons produced on the faces out of line-of-sight, and secondary electrons produced from chamber walls by stray backscattered electrons, are also detected.

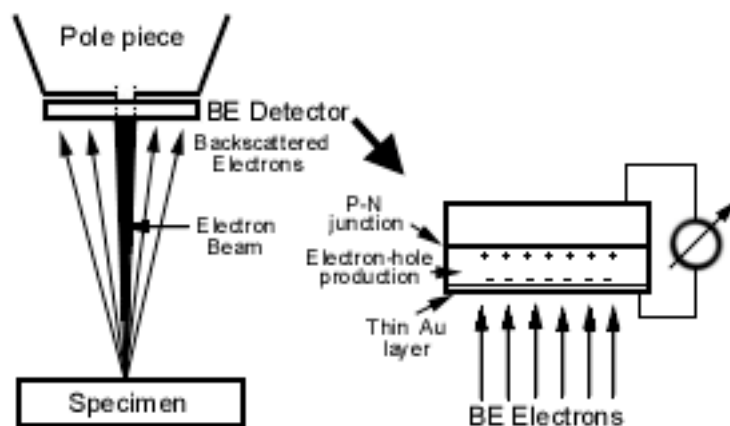


(A) negatively biased, (B) positively biased E-T detector, located near the top of the image

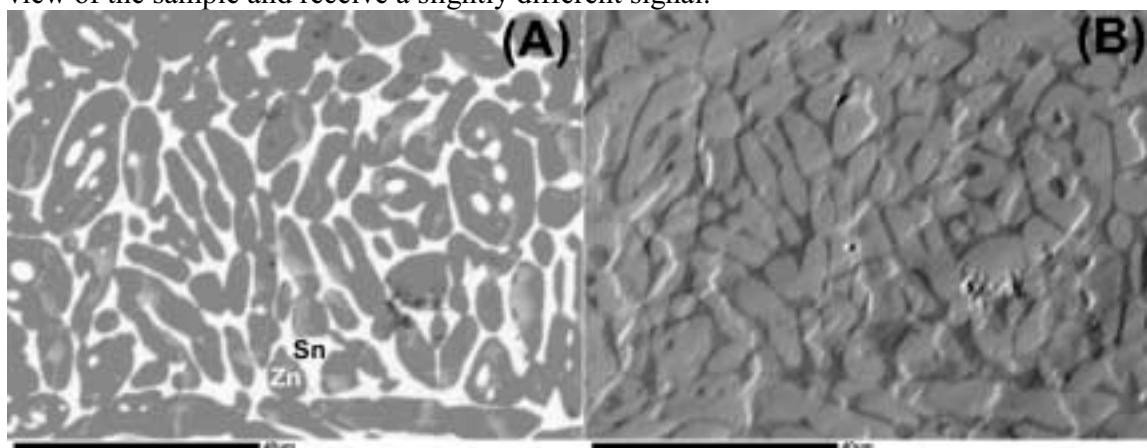
4.1.2 Solid-state diode detector for compositional contrast

This detector operates on the principle of electron-hole pair production induced in a semiconductor by energetic electrons. When the energetic backscattered electrons interact with the detector, a valence band electron may be promoted to the conduction band producing an electron-hole pair, which may be swept away by a bias applied to the detector. The generated current signal is then amplified and used to construct the scanning electron image.

The detector is a flat, annular, thin wafer placed on the polepiece of the objective lens. This location of the detector provides it with a large solid-angle for detection. The detector is sensitive only to the high energy backscattered electrons as the secondary electrons do not have the energy required to produce electron-hole pairs in the detector. Low energy backscattered electrons are also not detected. But since these electrons are produced by multiple scattering deep in the specimen, an image consisting of them will have a poor spatial resolution. Thus, the not detecting these electrons actually improves resolution.



The detector can operate either in a sum or a difference mode. The detector ring is split into two semi-circles, A and B. True compositional contrast is obtained in the sum (A+B) mode, where the signal from both parts of the detector are added. In a difference (A-B) mode, topographic contrast prevails because the two parts of the detector have a different view of the sample and receive a slightly different signal.

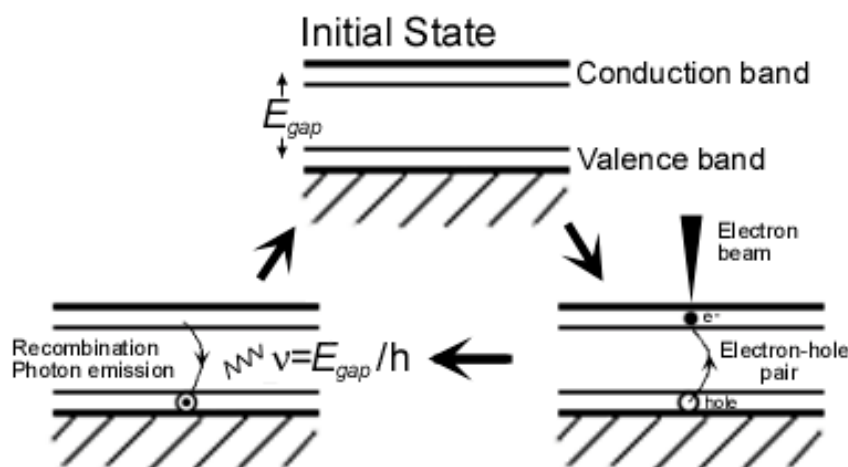


Scanning backscattered electron images of a Zn-Sn composite collected through a solid-state diode detector in (A) A+B, or compositional mode; (B) A-B, or topographic mode

4.2 CATHODOLUMINESCENCE DETECTOR

When certain materials, such as insulators and semiconductors, are bombarded by energetic electrons, long-wavelength photons are emitted in the ultraviolet, visible and infrared regions of the electromagnetic spectrum. This signal, known as cathodoluminescence, can be used to obtain a scanning cathodoluminescence (CL) image of

the specimen surface. Cathodoluminescent materials have a filled valence band and empty conduction band separated by an energy gap, E_{gap} , of forbidden energy states. When an energetic beam electron scatters inelastically, electrons from the filled valence band can be promoted to the conduction band each leaving a hole in the valence band, which creates an electron-hole pair. When the electron and the hole recombine, energy equal to E_{gap} is released as a photon. This energy, E_{gap} , is characteristic of the target material and can be used in its identification in a cathodoluminescence spectrum. Presence of trace amounts of impurity, however, shifts the energy and intensity of the peak as additional energy states become available in the band gap for transitions to occur.



CL can also be excited by x-rays generated in the sample. Hence, the volume of CL excitation can be slightly larger than the primary electron interaction volume. CL images often have poorer spatial resolution than scanning electron images. The reason is the greater depth of sampling by the CL signal, especially in bulk samples. In thin films, the resolution of CL images is better.

A CL detector consists of a parabolic mirror, mounted on a spectrometer port, and a light guide to collect and direct the emitted light into a photomultiplier. The signal from the photomultiplier may be dispersed through an optical spectrometer to record the CL spectrum, and select a wavelength to be used with an oscilloscope to obtain a scanning CL image. On the JEOL JXA-733, the optical microscope mirror may be combined with the photomultiplier used for secondary electron detection to create a simple setup for scanning CL imaging. This is done by removing the optical microscope eye-piece and attaching the photomultiplier tube, disconnected from the secondary electron detector port, in its place. In the absence of a light spectrometer, the entire spectrum of emitted light is used to obtain the scanning CL image.

4.3 X-RAY DETECTORS

An x-ray detector is usually a part of a spectrometer, either an energy dispersive spectrometer (EDS) or a wavelength dispersive spectrometer (WDS). Here, we discuss EDS in brief. We will discuss WDS in greater detail.

4.3.1 Energy Dispersive Spectrometer (EDS)

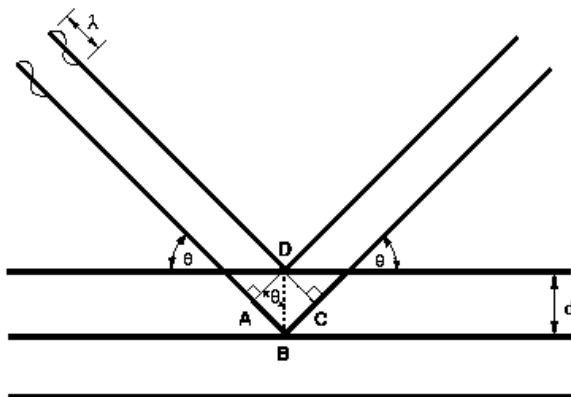
An energy dispersive spectrometer (EDS) takes advantage of the phenomenon of electron-hole pair production by energetic x-rays in semiconductors. X-rays emitted from the specimen are detected by a solid-state device which, after amplification, produces pulses proportional in height to the x-ray photon energy. A multichannel analyzer (MCA) is then used to sort the pulses into bins of a histogram to construct an x-ray spectrum. The detectors are usually made of lithium-drifted silicon (Si(Li)). Germanium detectors are also available and are useful for detection of higher energy x-rays (>20 keV). The x-ray spectrum covers the entire incident energy range (0 keV to E_0). However, the resolution is poor below 1 keV for a Si(Li) detector. Elements down to Be ($Z=4$) may be detected using a very thin window or a window-less detector.

Pure Si is an intrinsic semiconductor and is a good material for a detector. However, the purest available silicon contains some residual impurities such as B, causing it become a conductor. Boron creates holes in the valence band of Si as it has less number of valence electrons than Si, and the holes become the charge carriers. B is a p-type dopant. An n-type dopant such as Li or P adds an electron to conduction band as it has a larger number of valence electrons than Si. Hence, to counter the effect on the B impurity and create an 'intrinsic' condition, Li (an n-type dopant) is applied on the surface of a p-type Si crystal and allowed to diffuse into the crystal. This forms a few micrometer-thick p-n zone at the contact. This p-n zone serves as an intrinsic semiconductor. Later, most of the p-type material is removed from the surface of the Si-crystal exposing the p-n zone. A reverse bias is applied to the p-n zone, which enlarges the intrinsic zone to a few millimeters. It should be noted that Li is mobile in the presence of an applied field at room temperature. Hence, a Si(Li) detector should never be biased except near liquid-nitrogen temperatures to avoid permanent damage to the crystal.

4.3.2 Wavelength Dispersive Spectrometer (WDS)

A WDS setup consists of two parts: an analyzing crystal and a proportional counter. The latter serves as the x-ray detector. WDS takes advantage of the Bragg diffracting characteristics of an analyzing crystal to preferentially deflect the wavelength of interest toward the detector. Bragg's law is defined as follows:

$$n\lambda = 2d \sin \theta \quad (4.1)$$



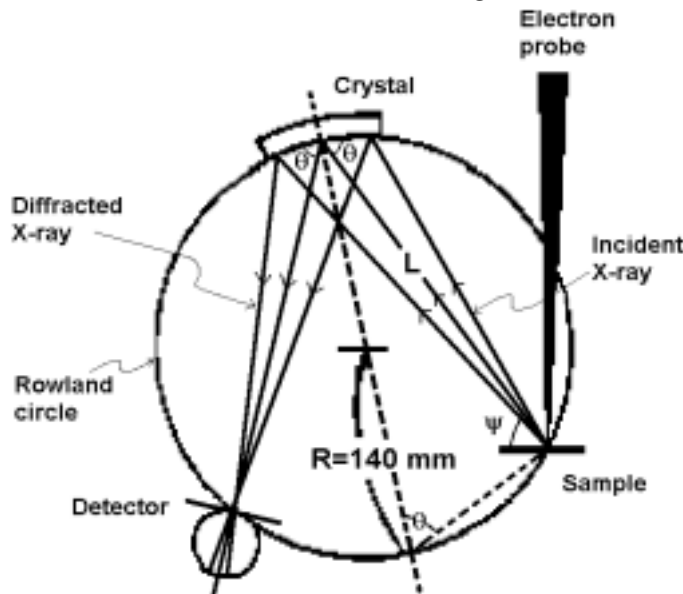
Diffraction according to Bragg's law. Strong scattering of x-rays of wavelength $n\lambda$ occurs at angle θ . At all other angles, scattering is very weak.

where, λ is the wavelength of the x-ray, d is the lattice spacing of the crystal, θ is the angle of incidence and diffraction and n is the order of reflection. X-ray waves, incident on the crystal, are reinforced after diffraction when the path lengths between two waves differ by an integral (n) of the wavelength. The effect of combined reflections from a large number of planes results in a relatively narrow intensity distribution around a peak. For example, the measured full-width, half-maximum (FWHM) for $\text{MnK}\alpha$ is about 10 eV, compared to the natural value of 2 eV.

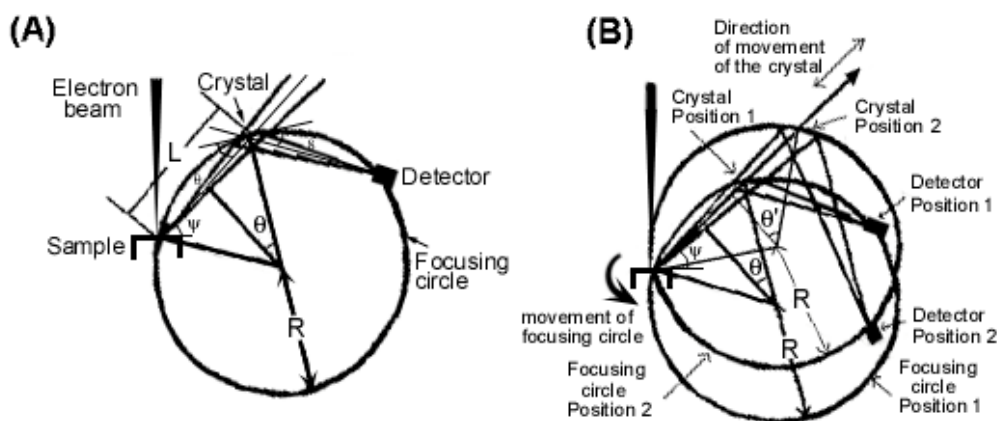
In a WDS spectrometer, the x-ray source (point where the electron beam strikes the sample), the analyzing crystal and the detector are constrained to be on a circle known as the focusing circle. In a Johansson type fully focusing spectrometer, the crystal is curved to a radius of curvature of $2R$ and then ground to R , so that its lattice planes and the focusing circle have the same curvature. This maximizes the diffracted x-ray signal at the detector. In reality, crystals are not ground as it degrades the resolution of the crystal. This compromise, known as Johann optics, does not seriously impair spectrometer resolution. From the geometrical configuration of the instrument, λ is related to L , the distance between the sample and the analyzing crystal by the following relation:

$$L = n\lambda.R/d \quad (4.2)$$

(mm), where, R is the radius of the focusing circle (140 mm in the JEOL JXA-733). The L values for different radiations of different elements are given in the JEOL L -value chart.



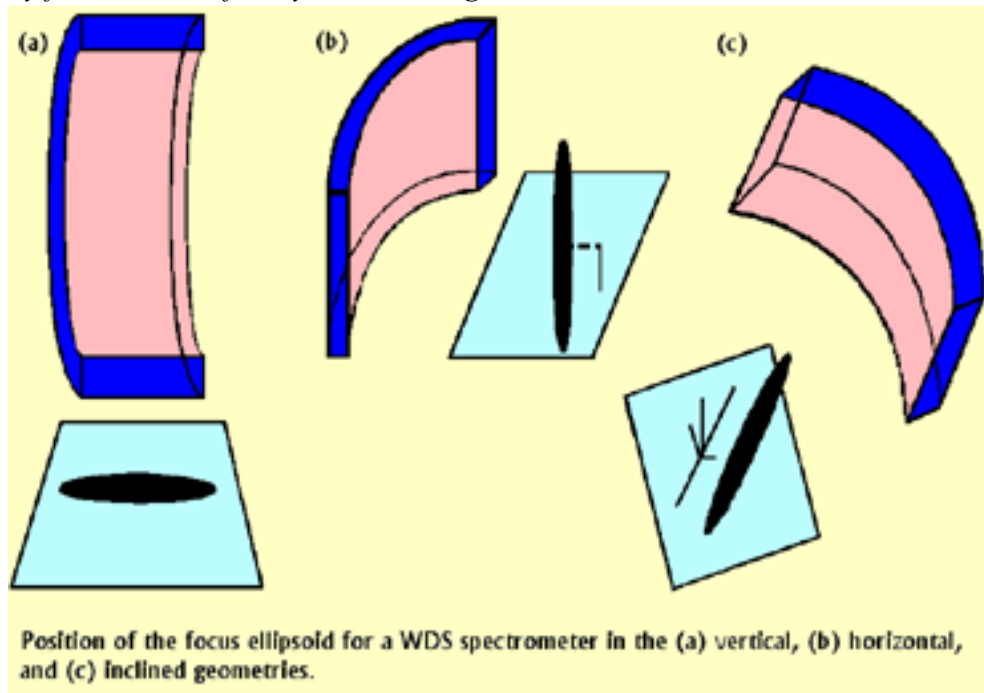
The crystal may be moved in a straight line toward or away from the sample while rotating it (to change θ , the incidence angle) to obtain reflections of other wavelengths. The direction of movement is fixed and establishes the take-off angle (ψ , the angle between the specimen-surface and the emergent x-ray traveling toward the analyzing crystal) of the x-rays. The detector moves simultaneously to make the focusing circle rotate about the point source.



Fully focusing wavelength dispersive spectrometer. R is the radius of the focusing circle, ψ is the take-off angle, and θ is the diffraction angle. Movement of the focusing circle to change the diffraction angle to θ' is shown in (b).

Because of the characteristics of a WDS spectrometer, only a finite volume of the sample is in focus: the WDS spectrometer has an elliptical view of the sample. This volume is usually an extremely elongated ellipsoid, whose major axis is proportional to the width of the diffracting crystal and has a length of millimeters. The minor axes are controlled by the sharpness of the diffracted peak and is on the order of micrometers. This ellipsoidal volume is important since any x-ray signal produced within it will be detected by the spectrometer.

Usually, WDS spectrometers are positioned vertically, that is, the focusing circle is vertical in an electron microprobe. In this configuration, the greatest sensitivity to spectrometer defocusing occurs along the Z (vertical) direction of the sample. In a horizontal configuration, the long axis of the ellipsoid is parallel to the Z direction, but at the expense of a large angle to the electron beam. This necessitates tilting of the specimen to obtain a useful take-off angle. The inclined spectrometer is a compromise between these two configurations. Note, however, that although the radius of the primary x-ray interaction volume is usually a few micrometers, the radius of the volume in which secondary fluorescence of x-rays occurs is about 10 times the primary radius. So, *in a vertically positioned WDS spectrometer, secondary fluorescence of x-rays cannot be ignored.*

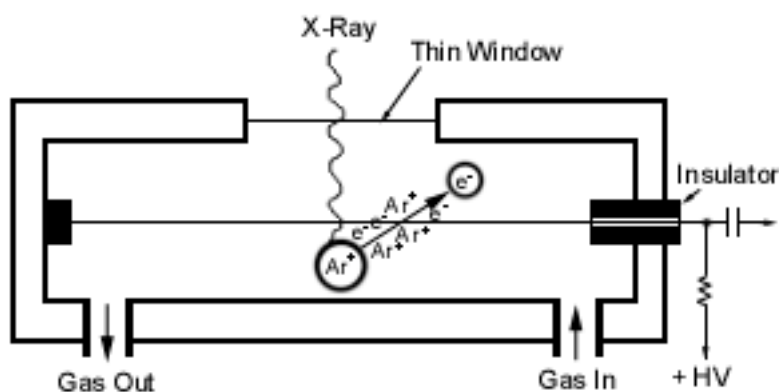


Focusing in an electron microprobe is usually achieved through a coaxial light microscope, which is prealigned with the electron optics. This light microscope has an extremely shallow focus. As a result, the surface of the sample can be focused accurately. To ensure that the appropriate axis of the focusing ellipsoid of the WDS spectrometer is in the same horizontal plane as the focused surface of the sample during routine alignment, the spectrometer is slowly moved up or down until the maximum x-ray count rate is observed for a certain element. The change in count rate is readily observed in a vertical spectrometer since it has the greatest sensitivity to spectrometer defocusing along the vertical direction.

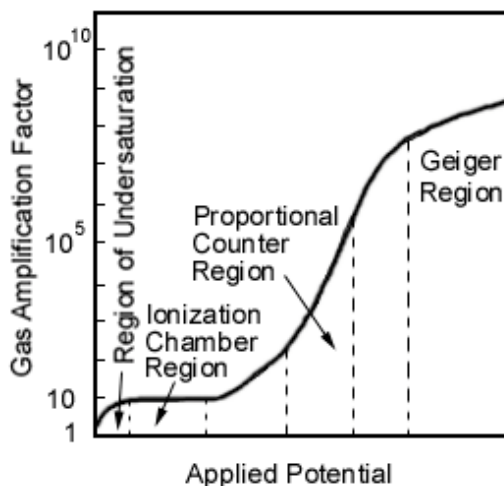
Analyzing crystals commonly available on the JEOL JXA-733 Superprobe and elements commonly analyzed with them are as follows:

Name	2d (Å)	Type	Resolution	Reflectivity	Elements usually analyzed
LDEC	98	Ni/C Layered Synthetic Microstructure	Low	High	B-O ($K\alpha$), optimized for C analysis
STE	100.4	Pb stearate	Medium	Medium	B-O ($K\alpha$), optimized for C analysis
LDE1	59.8	W/Si Layered Synthetic Microstructure	Low	High	C-F ($K\alpha$), optimized for O analysis
TAP	25.8	Thallium acid phthalate	Medium	Medium	Na-P ($K\alpha$); Cu-Zr ($L\alpha$); Sm-Au ($M\alpha$)
PET	8.742	Pentaerythritol	Low	High	S-Mn ($K\alpha$); Nb-Pm ($L\alpha$); Hg-U ($M\alpha$)
LIF	4.028	Lithium fluoride	High	High	Ti-Rb ($K\alpha$); Ba-U ($L\alpha$)

X-ray detectors in WDS: The commonly used detector in WDS spectrometers is a gas-proportional counter. It consists of a gas filled tube with a thin tungsten wire attached along the tube-axis, which is kept at a 1-3 kV potential. An x-ray photon enters the tube through a thin window and is absorbed by a gas atom. The atom is ionized and an electron is ejected, which in turn loses its energy by ionizing other gas atoms. The counter, thus, has an

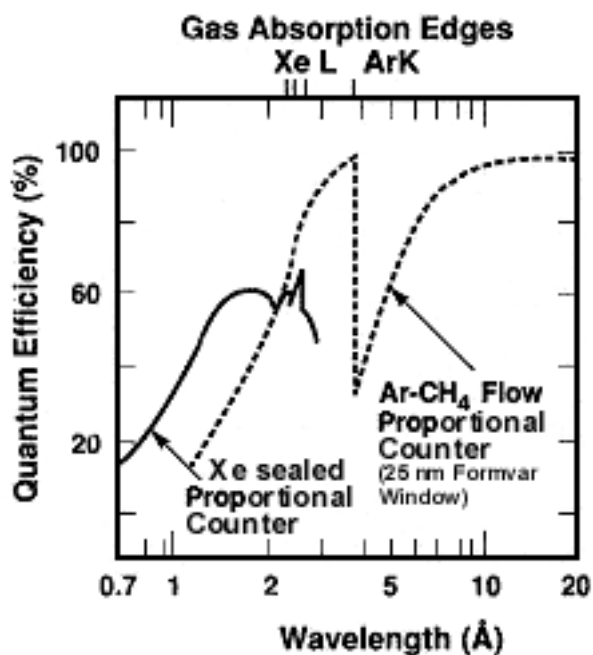


excellent dynamic range (0-50,000 counts per second). The electrons thus released are attracted by the central wire giving rise to a charge pulse. Since this is a very low energy pulse, the internal amplification by the gas (gas amplification factor) may be increased by increasing the potential in the wire. The gas amplification factor increases with the applied

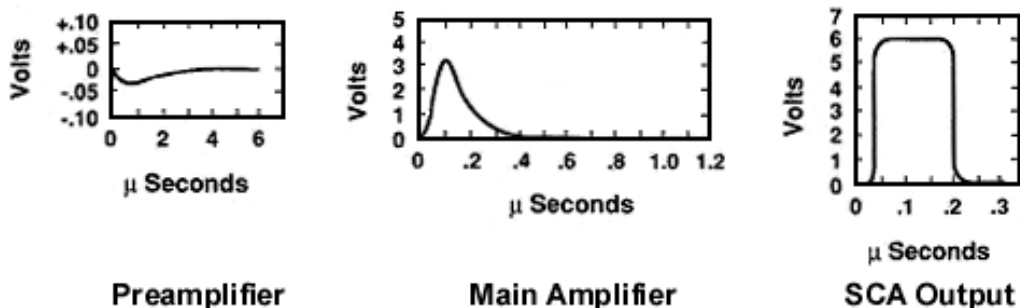


potential in three distinct stages: an ionization stage, a proportional stage and a Geiger stage. The proportional region is the most useful because the collected charge remains proportional to the energy of the incident x-ray photon.

The quantum efficiency, or the percentage of input pulses detected, depends on the gas used in the counter. In a flow-proportional counter, a mixture of 90% Ar and 10% CH₄ (P-10) flows through the tube. The window is usually made of Formvar or cellulose nitrate on a fine wire screen. This setup works well for long wavelength (low energy) x-rays. For shorter wavelengths, sealed-proportional counters containing Xe or Kr and a Be window are used. The efficiency of Ar-filled detectors may, however, be improved by increasing the gas pressure to 2-3 atmospheres.

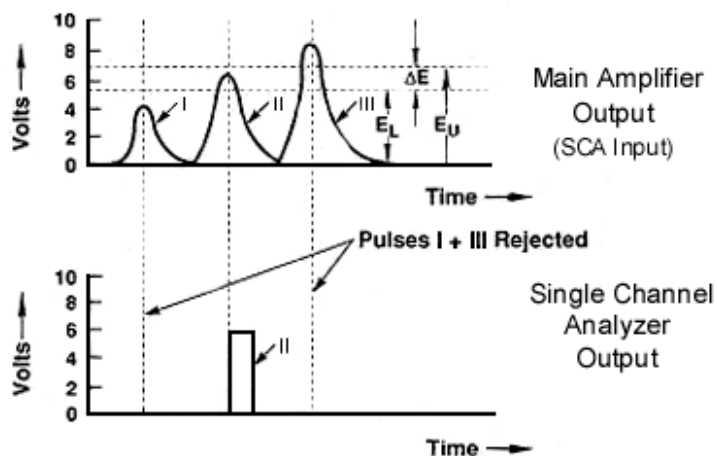


Pulse processing in WDS: After the charge is detected by the counter, it goes through a preamplifier to produce a voltage pulse. A typical preamplifier output pulse shape is a rapidly falling negative pulse with a tail a few microseconds long. This pulse then goes through the main amplifier, which inverts, amplifies and shapes it into a Gaussian pulse. The voltage of this output pulse depends on the gas amplification factor, the gains of the preamplifier and the amplifier and the capacitance of the preamplifier. If these quantities are held constant, the voltage of the pulse is directly proportional to the energy of the x-ray photon entering the proportional counter.



Typical WDS x-ray detection pulse shapes

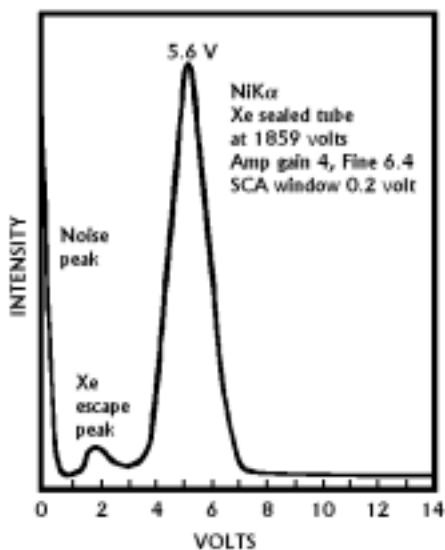
Output pulses from the amplifier now enter the single channel analyzer (SCA). An SCA serves two functions: it selects pulses within a predetermined voltage range, and it triggers rectangular pulses of a fixed voltage and duration compatible with scaler and rate-meter input requirements. Selection of pulses within a predetermined voltage range is called pulse-height analysis (PHA). The operator selects a baseline voltage, E_L , and a window voltage, ΔE , (differential setting), or only the baseline (integral setting). In the example shown in the figure, only pulses between 5 and 7 eV (pulse II) are accepted. In setting the



PULSE HEIGHT ANALYSIS

baseline and window voltages one must be careful of pulse shifts at higher count rates, which is observed for many metals. The reason for this phenomenon is not well known. In other words, the PHA settings are not guaranteed to work at different count rates.

In practice, the pulse-voltage distribution is obtained by selecting a small window voltage (ΔE of a few tenths of a volt) and moving the baseline over the whole SCA voltage range (0-10 V) at a fixed rate. A typical SCA scan shows a large noise peak near 0 V, an



Pulse distribution of NiK α determined by a single-channel analyzer

"escape peak" and the actual energy peak. The escape peak corresponds to an energy equal to the actual energy minus the characteristic energy of the detector gas (e.g., 2.96 keV for $\text{ArK}\alpha$). Escape peaks are produced when characteristic x-rays, generated by the detector gas (e.g. $\text{ArK}\alpha$), escape the counter, which results in a diminished energy equal to the initial energy entering the counter minus the energy lost through inner-shell ionization of the detector-gas.

The percentage resolution of a detector is the energy width of a peak at FWHM (full-width at half-maximum) divided by the mean peak energy multiplied by 100. A properly functioning counter tube has a resolution of about 15-20%. The pulse distribution should be approximately Gaussian and free of large asymmetric tails.

The energy resolution capability of the SCA scan may be used to select the energy of interest in case of peak-interferences. In WD spectrometry, however, the analyzing crystal always has a much better resolution than the SCA. Higher order Bragg reflections ($n>1$), however, can be efficiently eliminated by correctly setting the baseline and window voltages of the SCA. The SCA is also useful in eliminating low and high-energy noise.

An x-ray pulse needs a finite time interval to pass through the detector electronics. The time interval during which the detector is unavailable to subsequent pulses because of pulse processing is called dead-time. The corrected count rate, N , is given by $N/(1-\tau N)$, where N' is the measured count rate, and τ is the dead time. One method of determining τ consists of plotting N' versus the beam current, which is proportional to N . Any deviation of this plot from linearity can be fitted to the corrected count rate-expression to determine τ .

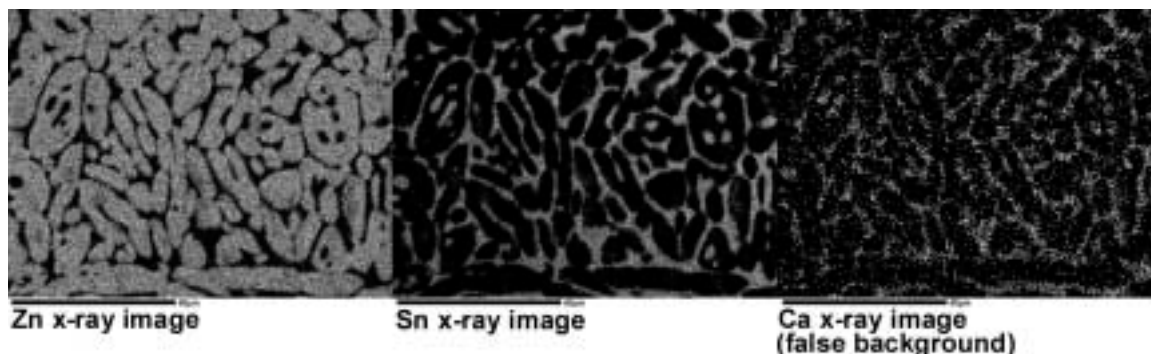
5. COMPOSITIONAL IMAGING BY WDS

Scanning x-ray images take advantage of the proportional counter output to provide elemental concentration information over an area in a graphical manner. The process is similar to the formation of a scanning electron image except for the difference in the signal. Analog dot-mapping is used to view quick qualitative elemental maps on the CRT. In this mode, the signal is converted into a binary form: 0, when the element is absent, and 1, when it is present. This is necessary because x-ray signals are typically weak compared to, for example, the electron signals.

Quantitative compositional x-ray images can be obtained by using longer dwell-time per point and higher beam currents. Depending on the dwell-time and the beam current used, an x-ray signal can be depicted on a grey scale only for relatively high concentrations (>25%). A beam current is chosen so that a count rate is about 100,000 counts/sec. In general, 10^5 - 10^6 x-ray pulses must be accumulated over the entire image field to obtain a high quality image.

Digital compositional images may provide a complete quantitative analysis at every pixel scanned. Each pixel intensity data is first corrected for background. Then, a k-ratio map is calculated by dividing each background-corrected pixel intensity data with a standard intensity. A single point intensity measurement on a standard is sufficient to calculate a k-ratio map. Because several WDS spectrometers are usually available on an electron microprobe, many images can be acquired simultaneously. If all the major elements are mapped, matrix corrections can be applied on each pixel k-ratio data to calculate a true quantitative compositional image.

Background correction. In true quantitative maps, the background intensities must be subtracted from the peak intensities on each pixel. Images not corrected for background contain a continuum artifact, which arises from the fact that the continuum is different for different phases with different mean atomic numbers. Thus, even if an element is absent in the sample, it might appear on a compositional map due to the atomic number dependence of the continuum.



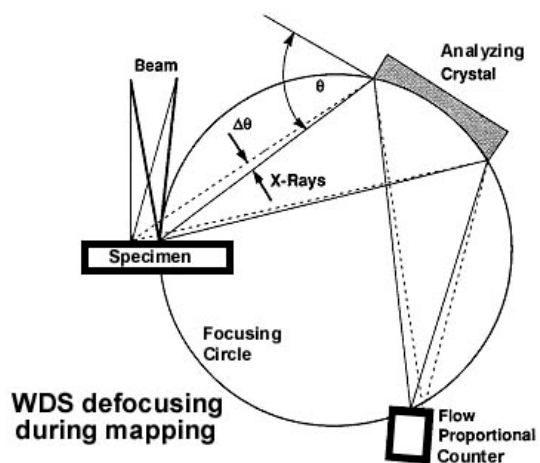
In WDS mapping, the conventional background measurement procedure by detuning the spectrometers is too time consuming and impractical. To solve this problem in a time-efficient way, the background is calculated using Kramer's equation:

$$I_{cm} \approx i\check{Z}(\lambda/\lambda_{swl}-1) \approx i\check{Z}(E_0-E_v)/E_v \quad (5.1)$$

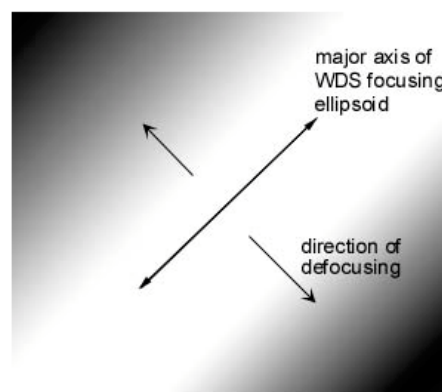
where, I_{cm} is the intensity of the x-ray continuum, i is the beam current, \check{Z} is the average atomic number, λ is the wavelength of interest corresponding to energy E_v , λ_{swl} is the short wavelength limit corresponding to the beam energy E_0 . Since \check{Z} is unknown, an iterative method must be used to calculate I_{cm} . The background is first measured with each WDS spectrometer on an element not present in the specimen. This first estimate is used to correct the measured intensities and calculate the major element concentrations, which in turn is used to calculate the mean atomic number. The background is recalculated using this mean atomic number. After three iterations, the background is calculated with sufficient accuracy.

5.1 Defocusing correction during WDS compositional imaging

The electron beam is typically scanned in a raster pattern, which causes deviation from a perpendicular incidence of the beam on the specimen surface. It may move off of the volume defined by the WDS focusing ellipsoid. Consequently, the Bragg condition for diffraction may not be maintained during a scan. The x-ray intensity falls sharply as the Bragg condition is lost. Bragg condition may, however, be maintained for beam positions on the sample that are parallel to the width of the diffracting crystal, i.e., along the direction of the WDS focusing ellipsoid. A band of high intensity may thus appear on the map with the intensity falling off on either side of the band. This defocusing effect is greater at lower magnifications because the beam deviates more from perpendicular incidence.



As the beam moves off the optic axis, the displacement in the specimen plane is equivalent to a change in the angle of incidence of the x-rays on the crystal by an angle $\Delta\theta$.



Example of a defocused image

There are four approaches to correct WDS defocusing (Newbury et al., 1990):

- *Stage scanning*: The beam is fixed and the specimen stage is scanned mechanically in the x-y plane. If necessary, it can also be moved in the z-direction with automatic focusing of the optical microscope. For low magnifications (<100X), this is the preferred mode of operation.
- *Crystal rocking*: The spectrometer crystal can be rocked in synchronism with the x-y scan to maintain accurate x-ray focus, i.e., the beam is always incident on the center of the WDS focusing ellipsoid. This is possible with full digital computer control.
- *Standard mapping*: The specimen and the standard can be scanned under the same conditions of magnification so the defocusing is identical in both maps. In a k-ratio map, calculated from the specimen and the standard maps, the defocusing effect cancels out. A homogeneous and featureless standard is required in standard mapping as any defects such as pits or scratches will appear in the k-ratio map.
- *Peak modeling*: An exact geometric correspondence exists between the shape of the defocusing response along a line perpendicular to the line of maximum spectrometer transmission (the high intensity band on the image). This may be used to calculate a correction factor for any beam position from a scan of the x-ray peak.

6. QUANTITATIVE ANALYSIS BY WDS

For qualitative analysis of specimens (including powders), conductive mounting tapes may be used. A small piece or a few grains are mounted on a slide using double-sided sticky carbon tape. This may be loaded in the instrument directly and analyzed. For precise WDS analysis, however, careful sample preparation is essential. The sample should be cut to the size that will fit in one of the standard sample holders of the electron microprobe. Brittle samples and powders may be mounted in epoxy resin in the shape of 0.75" or 1" diameter pellets. The sample, or the mount, should be carefully polished: first with coarse SiC-paper or grit, and then with fine diamond or corundum (Al_2O_3) grit. The final grit size should be at least 0.25μ , and preferable 0.06μ . The polished sample should then be cleaned properly to

get rid of any polishing grit and other surface contamination by ethyl alcohol or distilled water using an ultrasonic cleaner. Finally it should be completely dried using an "environment-safe" duster, or leaving it in a 100°F oven for a few minutes.

Electrically non-conductive samples are routinely carbon-coated to ensure conduction of the beam electrons away from the sample. Conductive samples need not be coated. However, if they are mounted in a non-conductive material, carbon-coating is recommended. The standards and the sample should be coated to the same thickness. Carbon coating is carried out by carbon evaporation under vacuum. A polished brass block is used to monitor the thickness of carbon coat deposited on the specimens. As the thickness of coat increases on the brass, it changes color from orange (150 Å) to indigo red (200 Å), then to blue (250 Å), and then to bluish green (300 Å). A thickness of 225-250 Å is recommended for microprobe analysis at 15-20 keV accelerating voltage.

Quantitative analysis by WDS requires prior knowledge of which elements are present and to be measured in the sample. This requires qualitative analysis. Qualitative analysis by WDS is time consuming as it requires scanning each spectrometer over its entire wavelength range to see which peaks are present. In a complex sample, this would mean scanning through hundreds of peaks because WDS has a fine energy resolution. Energy dispersive spectrometry (EDS), on the other hand, is a quick way of obtaining a qualitative spectrum. The EDS software is usually equipped with a KLM line marker database, which is very useful in peak identification. One should, however, be careful of trace elements (low peaks) and peak overlaps. Depending on the type of window, the EDS detector can detect elements above a certain atomic number. With a commonly used Be window, one can detect elements only above atomic number 9 (F). Hence, it is not possible to determine whether the unknown is a metal-alloy or an oxide. Wavelength scans over a short range of wavelength, using a light element analyzing crystal (e.g., LDE1 or LDEC) may be used to qualitatively identify F, O, N, C and B. WDS scans are also used to detect trace elements.

Standard intensity calibration. Standard x-ray intensities of the elements to be measured are obtained on appropriately chosen standards. Different standards may be used for different elements. The user must decide which WDS spectrometer should be used to measure the intensity of a particular x-ray line ($K\alpha$, $L\alpha$, etc.) of an element. Secondary standards may be analyzed as unknowns to check if their known compositions are reproduced. The analytical conditions (e.g., accelerating voltage, beam current, etc.) are maintained throughout the session.

Measurement of X-ray intensities in the specimen. X-ray intensities of the elements under consideration are obtained in the specimen under the same analytical conditions. The user must decide on the counting time for each element. Usually longer counting times are used for trace elements, which improves counting statistics. K-ratios are calculated by dividing the measured intensities by the corresponding standard intensities.

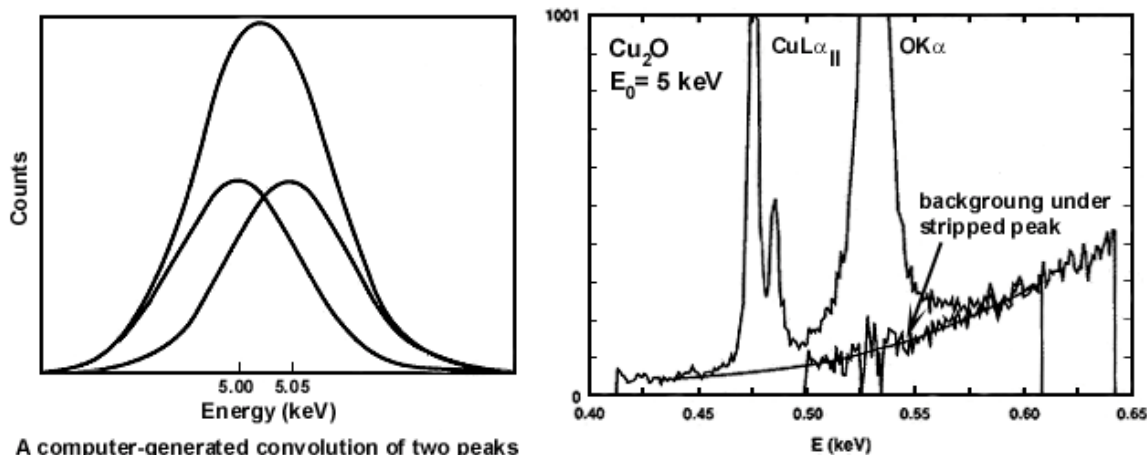
Both the standard intensity and the intensity on the specimen must be corrected for background and should be free of overlaps. The usual method to obtain background intensities is by interpolation. The spectrometer is set to measure count rates on two background positions on either side of a peak and the background under the peak is calculated by interpolating between the two measured values. Another way of obtaining the background is by measuring the intensity on a "blank" sample, which has approximately the same mean atomic number as the sample, but does not contain the element being measured. The spectrometer need not be moved to an off-peak position if background is measured by this method.

Data reduction through matrix correction. The measured x-ray intensities are reduced through a matrix correction scheme such as ZAF or $\phi(\rho z)$ to obtain weight percent concentrations of each element in the specimen.

6.1 Background and Peak Overlap Correction in WDS

The natural energy distribution of a characteristic x-ray line can be described by a Lorentzian probability function. The peaks recorded in WDS or EDS are a convolution of the natural peak and the instrumental response function. In EDS, the peaks are usually broad due to a large instrumental effect. Because of good spectral resolution in WDS, the natural Lorentzian shape is retained in most cases. In WDS equipped with layered synthetic microstructures (LSM) to measure light elements (e.g., LDE1 or LDEC), however, the peaks are broad and have a near-Gaussian shape.

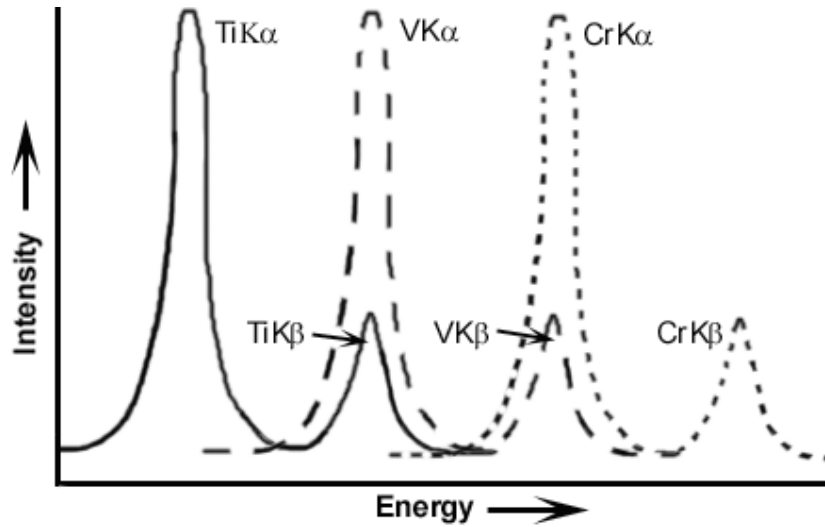
When a peak is broad, an overlap between adjacent peaks is possible. A broad peak may be the result of a convolution of two or more spectral peaks. Even when the Lorentzian shape is preserved, the tails of two adjacent peak may overlap because Lorentzian curves have long tails. When broad overlapping peaks are present in the spectrum, background modeling or filtering methods can be used to obtain the background intensities, and linear or



non-linear peak deconvolution methods can be used to subtract the effects of interfering peaks. Background modeling involves modeling the bremsstrahlung on the basis of the equations of continuum x-ray generation. Background filtering involves Fourier transform methods to filter out the background noise, once it has been identified over a large part of the spectrum (e.g., an EDS spectrum). Peak deconvolution methods involve characterization of simple one-element spectra and using them to strip peaks of interfering elements from the spectrum. One way of peak stripping is by multiple linear least-squares curve fitting.

In case of peak overlaps in convoluted narrow peaks (e.g., with the PET or LIF analyzing crystals), the magnitude of an overlap can be calculated by measuring the intensity of the overlapping peak on a standard that does not contain the element whose peak is being overlapped. Let us consider the Ti-V-Cr system. There are two significant peak overlaps in the x-ray spectrum of a Ti-V-Cr alloy. The $\text{VK}\alpha$ and the $\text{CrK}\alpha$ peaks are overlapped by the $\text{TiK}\beta$ and $\text{VK}\beta$ peaks respectively. The intensity contributions from the $\text{TiK}\beta$ and $\text{VK}\beta$ peaks must be subtracted from the measured intensities of $\text{VK}\alpha$ and $\text{CrK}\alpha$ in order to obtain

the true intensities of $VK\alpha$ and $CrK\alpha$. Following is a schematic representation of the x-ray spectrum of a Ti-V-Cr alloy:



This makes the measured intensities of $VK\alpha$ (in the presence of Ti) and $CrK\alpha$ (in the presence of V) to be higher than true intensities, specially when V or Cr are in present only in trace amounts in the sample. The intensities of the $VK\alpha$ and the $CrK\alpha$ x-rays may be corrected according to the following equations:

$$I_{VK\alpha}^{corr} = I_{VK\alpha}^{meas} - \frac{I_{TiK\alpha}^{meas}}{I_{Ti-std}} I_{VK\alpha}^{Ti-std} \quad (6.1)$$

$$I_{CrK\alpha}^{corr} = I_{CrK\alpha}^{meas} - \frac{I_{VK\alpha}^{corr}}{I_{V-std}} I_{CrK\alpha}^{V-std} \quad (6.2)$$

where, I stands for intensity, "corr" for corrected, "meas" for measured and "std" for standard. $I_{VK\alpha}^{corr}$ in Eqn. 54, is calculated from Eqn. 53. To correct the intensity of $Vk\alpha$, the intensity of $Vk\alpha$ is measured on a pure Ti standard ($I_{VK\alpha}^{Ti-std}$). Since the pure Ti standard does not contain any V, the measured intensity of $Vk\alpha$ is entirely due to the contribution from $TiK\beta$. This intensity ($I_{VK\alpha}^{Ti-std}$) is subtracted from the $Vk\alpha$ intensity measured in the specimen ($I_{VK\alpha}^{meas}$) after scaling it ($I_{VK\alpha}^{Ti-std}$) down by a factor equal to the k-ratio of $TiK\alpha$ ($=I_{TiK\alpha}^{meas} / I_{TiK\alpha}^{Ti-std}$) in the specimen. The correction for $CrK\alpha$ is similar, except the corrected intensity of $Vk\alpha$ ($I_{VK\alpha}^{corr}$) is used instead of the measured intensity ($I_{VK\alpha}^{meas}$).

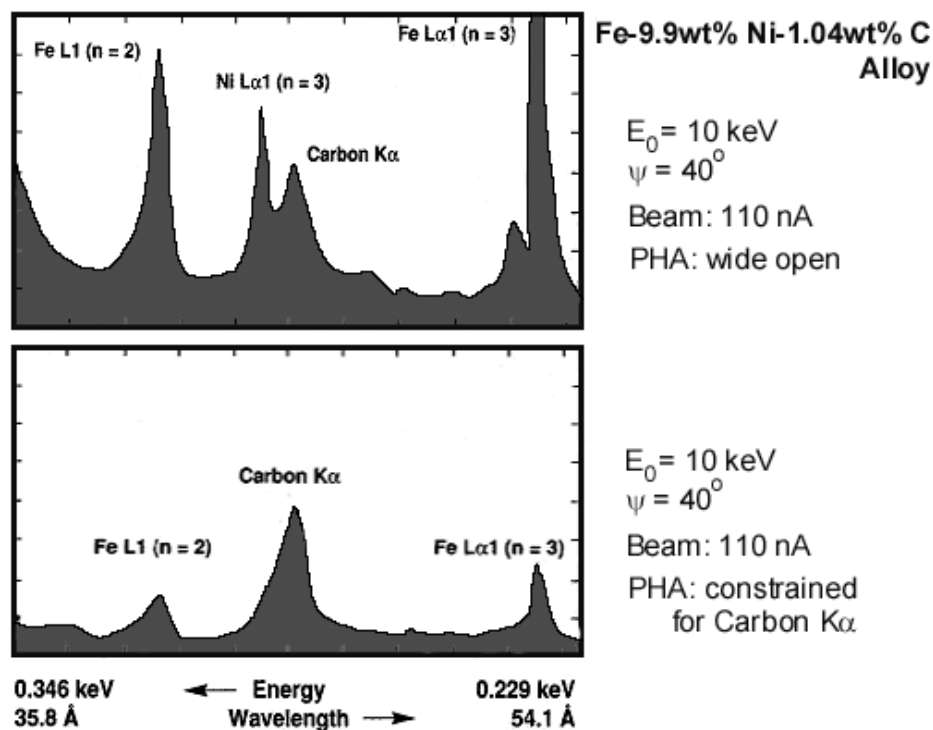
6.2 Light element analysis by WDS

The light elements F, O, N, C, B and Be present a special challenge for analysis by WDS. Special precautions and procedures are often employed while analyzing these

elements. Problems associated with light elements and possible solutions are discussed below.

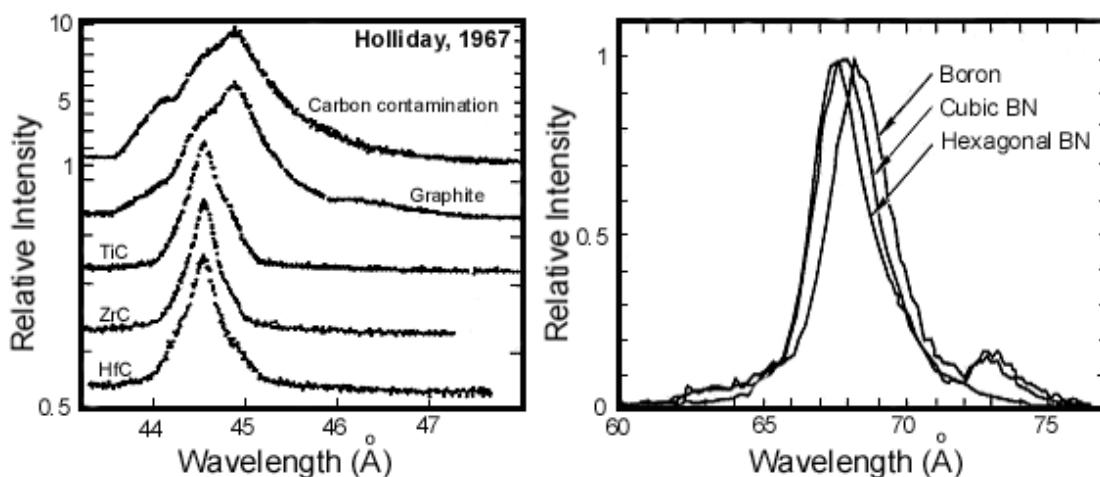
Interference by higher order metal lines. The transition metals Ti, V, Cr, Mn, Fe, Co and Ni, and the metals Zr, Nb and Mo emit x-rays at wavelengths similar to the characteristic wavelengths of the light elements. The last three elements also have absorption edges, which greatly diminish the emitted intensities of the light elements. For example, the $NK\alpha$ (31.6 Å) is severely overlapped by the $TiL1$ (31.4 Å) line. It is thus extremely difficult to measure N in the presence of Ti, specially if it is in trace amounts. In this case, the only way to analyze N is to use a known and well characterized TiN standard.

Correctly setting the PHA baseline and window voltages can often filter out the metallic higher order x-ray wavelengths. This is demonstrated in the case of carbon analysis in steel in the following wavelength scans, in which the higher order lines of Fe and Ni are efficiently subdued with PHA settings for carbon $K\alpha$:



It is always good to check if there is a pulse-shift in the PHA, going from the standard to the specimen when using narrow PHA window settings. If pulse-shift cannot be avoided, WDS peak fitting methods must be employed.

Chemical bonding shifts. In light elements, characteristic x-rays are generated when there is a transition of a valence electron to an empty K-shell. Since energy levels associated with valence electrons are highly affected by chemical bonding, characteristic wavelengths, intensities and peak shapes often shift depending on the nature of the bonding. The intensity of $BK\alpha$ actually also depends on crystallographic orientation. Following figures demonstrates peak shifts and peak shape differences among different carbides and among different B compounds:



In case of bonding related peak shifts, the integral intensity under the peak must be measured instead of the simple peak intensity. This is a time consuming process involving detailed WDS scans. Bastin & Heijligers (1984, 1986) devised the area peak factor (APF) analysis method to overcome this problem. APF is the ratio of the integral k-ratio to the normal k-ratio. They measured the APF for different light element compounds using different standards and created a database (Bastin & Heijligers, 1990, 1991). APF for $CK\alpha$ in different carbides using a Fe_3C standard are shown below as a function of the mean atomic number. APF values range between 0.7 and 1.1 with the strong carbide formers showing low values.

It should be noted that APF's depend on the spectrometer and the standard used.

Table: Area Peak Factor for $CK\alpha$ relative to Fe_3C

Carbide	Area Peak Factor for $CK\alpha$
B_4C	1.05
SiC	0.86
TiC	0.72
V_2C	0.77
VC	0.78
$Cr_{23}C_6$	0.80
Cr_2C_3	0.81
Cr_3C_2	0.83
Fe_3C	1.00
ZrC	0.71
NbC	0.79
Mo_2C	0.83
HfC	0.84
TaC	0.97
WC	0.98
W_2C	1.03

Note: measured with a STE crystal at 10 keV and 300 nA
(approximate values from Bastin & Heijligers, 1991)

Hence, they must be determined on the instrument being used. There are indications, however, that APF's determined on similar instruments are within experimental errors.

Choice of standards. The rule of thumb is to choose a standard as similar as possible to the specimen. The standard should yield reproducible intensities. For example, graphite

does not yield reproducible intensities for $CK\alpha$ and is not a good standard for C. Fe_3C is recommended as a standard for C analysis in steel.

Surface carbon contamination and carbon-coating. Most electron microprobes are pumped by oil-based pumps. Organic (oil) molecules floating inside the sample chamber are deposited and polymerized on the sample by the action of the electron beam. $CK\alpha$ intensity is found to increase with time when the beam is left on the same spot and no precaution is taken. If an air-jet is used to blow away the organic molecules from the surface of the sample contamination can be avoided. A liquid nitrogen cold trap near the sample also helps to reduce the contamination.

Since carbon highly absorbs low energy x-rays, surface carbon contamination may affect other light element analysis as well. For the same reason, carbon-coating of non-conductive sample greatly reduces characteristic x-ray intensities of other light elements. Other coating material may be used in such a case. For carbon analysis in non-conductive specimens, Al coating has been suggested.

Background measurement. Finding the background by interpolation of two measurements on the two sides of a peak may be dangerous for light elements because the background is rarely straight and flat. It is always recommended to do a wavelength scan to determine the positions where backgrounds can be measured safely. Alternatively, samples similar to the specimen, but without the light element of interest ("blank" samples), may be used to measure background. Non-linear peak stripping methods may be used to delete peak overlaps.

Large absorption corrections. The matrix correction models are severely tested while calculating concentrations of light elements from measured k-ratios. This is because light elements have very high mass absorption coefficients, many of which are not determined accurately. Variations of 100% are not uncommon between different studies. Bastin & Heijligers (1991) created a database of absorption coefficients from new measurements and best-fits of older measurements. Using their data it is possible to determine light element concentrations through the $\phi(\rho z)$ correction procedure. The PDH-

ZAF correction is not appropriate as it assumes a ϕ_0 of zero, whereas, most of the light element x-rays are generated close to the surface.

It is always recommended to use a low beam energy and a high take-off angle to minimize absorption effects. Beam energies in the range 5-15 keV may be used. 10 keV is appropriate in most cases. Higher beam currents (100-300 nA instead of the usual 10-30 nA) may be used to boost the signal. But this may lead to high dead times in the other spectrometers measuring metals. In case of high dead times, metals should be measured separately using appropriate analyzing conditions.

Use of layered synthetic microstructures. LSM's are routinely used in modern WD spectrometers for light element analysis. They provide high count rates and high peak/background ratios and are not very sensitive to metallic higher order reflections. In addition, flow-proportional counters with a high amplifier gain are used to make the counting process more efficient.

7. COMPARISON OF WDS AND EDS

The EDS and the WDS techniques have unique characteristics that complement each other during an analysis. Following is a comparison of the major features of the two methods.

Efficiency of x-ray detection: The geometrical collection efficiency of WDS is limited because of the Bragg focusing requirements and Johan optics. The EDS detector is usually placed close to the sample and has a larger collection efficiency. The maximum collection efficiency of WDS is ~0.2%, whereas, for EDS, it is ~2%.

Quantum efficiency, or the percentage of x-rays entering the spectrometer which are counted, is excellent and almost 100% in the 2.5-15 keV energy range for the solid-state EDS detector. For WDS, it is only about 30% because of losses by absorption in the analyzing crystal and the counter tube.

In EDS, only one detector is needed to collect the entire spectrum. In WDS, at least three or four spectrometers are needed as each analyzing crystal has a range of delectability. The EDS is very quick for a qualitative analysis. In WDS, the spectrometers have to scanned over a range of wavelengths to obtain a spectrum and is very time consuming.

Spectral resolution: A WDS system is excellent in terms of spectral resolution, which is of the order of a few electron volts, measured at FWHM. Peak-to-background ratios are high and there are rarely major peak-overlap problems. Pulse height analysis further removes higher order reflections. In comparison, the resolution of EDS detectors typically range 80-180 eV depending on the x-ray energy, and thus the peaks are considerably broader. The effect is to introduce peak-overlaps and reduce the peak-to-background ratio, which must be calculated by integration under the peak. Compared to WDS, where peak-to-background ratios may be of the order of 1000:1, corresponding ratios in EDS are approximately 100:1. The detection limit, a function of peak-to-background ratio, is given by,

$$C_{MDL} = \frac{3\sqrt{I_B / t}}{I_0} \quad (7.1)$$

where, C_{MDL} is the minimum detectable limit, I_B , the background intensity, I_0 , the net intensity (peak minus background) and t , the counting time (seconds). Thus, the minimum detectable limits for EDS are typically an order of magnitude higher than for WDS.

Maximum count rate and minimum probe size. Count rates are much lower in EDS because of dead-time accumulated during pulse pile-up rejection. The maximum count rates obtained with an efficiently operating EDS is about 2000 to 3000 cps over the entire range of excited x-rays. In WDS, count rates in excess of 50,000 cps on a peak are possible without loss of energy resolution.

The count rate depends on the probe current, which depends on the probe size. Since an EDS operates efficiently at lower count rates, the probe current can be lowered, which in turn decreases the probe size. This may seem to improve the spatial resolution for chemical analysis. However, spatial resolution actually depends on electron beam scattering and the interaction volume in the sample and does not improve much below 0.5 μm probe diameter. The EDS counters this problem by placing its detector closer to the sample, thereby increasing the x-ray collection efficiency and offsetting the loss from the use of a lower probe current. The minimum useful probe size is $\sim 2000 \text{ \AA}$ for WDS and $\sim 50 \text{ \AA}$ for EDS.

Stability. WDS systems are unstable over long terms due to wear and tear of mechanical components leading to backlash and small but significant deviations from exact Bragg focusing conditions. In addition, the analyzing crystals may slowly deteriorate. Temperature and pressure conditions in the counter gas may also change, affecting the efficiency of x-ray detection. EDS systems are not subject to mechanical wear. Detector efficiency may be reduced, however, owing to deposition of contaminants on the detector window. Moreover, vacuum in the detection system may deteriorate gradually, causing electronic noise and loss of resolution. Drift in electronics, such as change in amplifier gain, will also affect the analysis as peaks will be displaced in the spectrum.

Analysis results are usually not affected if measurements are taken sequentially on standards and specimens in the course of each session. It is risky to rely upon 'standardless' methods or reference to stored standard data.

Spectral artifacts. The EDS is subject to a number of detection artifacts including peak broadening, distortions, Si escape peaks, absorption and the Si internal fluorescence peak; pulse-processing artifacts including pulse pile-up, sum peaks and errors in dead time correction; and other artifacts arising from microphonics, ground loops, oil and ice contamination, and susceptibility to stray radiation because of a larger solid angle of collection. The WDS is relatively free of these artifacts.

8. REFERENCES

- Anderson, C.A. and Hasler, M.F. (1966) In *Proc. 4th Intl. Conf. On X-ray Optics and Microanalysis* (R. Castaing, P. Deschamps and J. Philibert, eds.) Hermann: Paris, p. 310.
- Bambynek, W., Crasemann, B., Fink, R.W., Freund, H.U., Mark, H., Swift, S.D., Price, R.E. and Rao, P.V. (1972) *Rev. Mod. Phys.*, 44, 716.
- Bastin, G.F. and Heijligers, H.J.M. (1984) In *Microbeam Analysis-1984* (A.D. Romig Jr. and J.I. Goldstein, eds.), 291.
- Bastin, G.F. and Heijligers, H.J.M. (1986) *X-ray Spectrom.*, 15, 143.
- Bastin, G.F. and Heijligers, H.J.M. (1990a) *Quantitative electron probe microanalysis of carbon in binary carbides*, Internal Report, Eindhoven Univ. of Technology.
- Bastin, G.F. and Heijligers, H.J.M. (1990b) *Scanning*, 12, 225.
- Bastin, G.F. and Heijligers, H.J.M. (1991) In *Electron Probe Quantitation* (K.F.J. Heinrich and D.E. Newbury, eds.), Plenum Press: New York, 145 and 163.
- Bearden, J.A. (1964) "X-ray Wavelengths", Report NYO 10586, U.S. Atomic Energy Commission, Oak Ridge, Tennessee.
- Bence, A.E. and Albee, A. (1968) *J. Geol.*, 76, 382.
- Berger, M.J. and Seltzer, S.M. (1964) *Nat. Acad. Sci./Nat. Res. Council Publ.* 1133, Washington, 205.
- Bethe, H. (1933) In *Handbook of Physics*. Springer: Berlin, 24, 273.
- Castaing, R. (1951) Ph.D. Thesis, University of Paris.
- Duncumb, P. and Reed, S.J.B. (1968) In *Quantitative Electron Probe Microanalysis* (K.F.J. Heinrich, ed.), *Nat. Bureau Stand. Spl. Publ.* 298, 133.
- Duncumb, P. and Shields, P.K. (1966) In *The Electron Microprobe* (T.D. McKinley, K.F.J. Heinrich and D.B. Wittry, eds.), Wiley: New York, p. 284.
- Evans, R.D. (1955) *The Atomic Nucleus*. McGraw-Hill: New York.
- Green, M. and Cosslett, V.E. (1961) *Proc. Phys. Soc., London*, 78, 206.
- Heinrich, K.F.J. (1969) National Bureau of Standards, Technical Note 521.
- Heinrich, K.F.J. (1986) In *Proc. 11th Intl. Conf. on X-ray Optics and Microanalysis* (J.D. Brown and R.H. Packwood, eds.), Univ. Western Ontario, London, Ont. Canada, p. 67.
- Holliday, J.E. (1967) *Norelco Reporter*, 14, 84.
- Joy, D.C. and Luo, S. (1989) *Scanning*, 11, 176.
- Kanaya, K. and Okayama, S. (1972) *J. Phys. D.: Appl. Phys.*, 5, 43.
- Myklebust, R.L., Fiori, C.E. and Heinrich, K.F.J. (1979) *Nat. Bureau Stand. Tech. Note* 1106.
- Myklebust, R.L., Newbury, D.E. and Marinenko, R.B. (1989) *Anal. Chem.*, 61, 1612.
- Newbury, D.E., Fiori, C.E., Marinenko, R.B., Myklebust, R.L., Swyt, C.R. and Bright, D.S. (1990) *Anal. Chem.*, 62, 1159A and 1245A.
- Packwood, R.H. and Brown, J.D. (1981) *X-ray Spectrom.*, 10, 138.

- Philibert, J. (1963) In *Proc. 34th Intl. Symp. X-ray Optics and X-ray Microanalysis, Stanford University* (H.H. Pattee, V.E. Cosslett and A. Engstrom, eds.) Academic Press: New York, p. 379.
- Pouchou, J.L. and Pichoir, F. (1984) *Rech. Aerosp.*, 3, 13.
- Powell, C.J. (1976a) *Rev. Mod. Phys.*, 48, 33.
- Powell, C.J. (1976b) In "Use of Monte Carlo Calculations in Electron Probe Microanalysis and Scanning Electron Microscopy" (K.F.J. Heinrich, D.E. Newbury and H. Yakowitz, eds.) National Bureau of Standards, Spl. Publ. 460, p. 97.
- Reed, S.J.B. (1965) *Br. J. Appl. Phys.*, 16, 913.
- Shimizu, R., Kataoka, Y., Ikuta, T., Koshikawa, T. and Hashimoto, H. (1976) *J. Phys. D.: Appl. Phys.*, 9, 101.
- Takakura, M., Notoya, S. and Takahashi, H. (2001) Application of cathodoluminescence to EPMA. *JEOL News*, 36E/1, 35-39.
- Thomas, P.M. (1964) U.K. Atomic Energy Auth. Rept. AERE-R 4593.
- Yakowitz, H., Myklebust, R.L. and Heinrich, K.F.J. (1973) *Nat. Bureau Stand. Tech. Note* 796.

8.1 Sources and Recommended reading

- 1) Reed, S.J.B. (1996) *Electron Microprobe Analysis and Scanning Electron Microscopy in Geology*. Cambridge Univ. Press: Cambridge, U.K.
- 2) Scott, V.D., Love, G. and Reed, S.J.B. (1995) *Quantitative Electron-Probe Microanalysis* (Second Edition). Ellis-Horwood: New York.
- 3) Goldstein, J.I., Newbury, D.E., Echlin, P., Joy, D.C., Romig, A.D.Jr., Lyman, C.E., Fiori, C. and Lifshin, E. (1992) *Scanning Electron Microscopy and X-ray Microanalysis: A Text for Biologists, Material Scientists, and Geologists* (Second Edition). Plenum Press: New York.
- 4) JEOL technical manuals.

8.2 Acknowledgements

The text book by Goldstein et al. (item 3 in above section) has been extensively used in preparing these notes. Most of the figures are from this book, but have been altered to suit the needs of this course. One of the figures in section 4.3 is based on a figure in the JEOL technical manuals. dQuant32 and dPict32 (section 9.2) are quantitative analysis and imaging programs developed by Chuck Herrington at Geller MicroAnalytical Laboratories.

9. THE MIT ELECTRON MICROPROBE FACILITY

The MIT electron microprobe facility consists of two JEOL JXA-733 Superprobes. Probe-A has five wavelength dispersive spectrometers (WDS) and Probe-B has four. Each is equipped with an energy dispersive spectrometer (EDS), a backscattered electron (BE) detector and a secondary electron (SE) detector. Two of the WDS spectrometers in Probe-A and one in Probe-B are fitted with layered synthetic microstructure diffractors for high quality light element (B,C,N,O and F) analysis. Each electron microprobe is automated by a Tracor Northern TN-5600 programmable automation controller (PAC). The PAC controls the stage, the WD spectrometers and the electron beam. The PAC itself is controlled by a master computer, a PC run by Windows NT, which serves as the user interface. The PCs are connected to the MIT-net through fast ethernet adapters. The program for quantitative analysis (dQuant32) and imaging (dPict32) are developed at Geller MicroAnalytical Lab by Chuck Herrington. The EDS analytical program is called Quantum-X, developed by American Nuclear Systems, Inc. The analysis data are stored in text files, which can be opened in a spreadsheet such as Excel. Both scanning electron (backscattered or secondary) and elemental scanning x-ray images of the specimen may be obtained. Scanning cathodoluminescence images may also be obtained. The elemental scanning x-ray images may be acquired both through WDS and EDS. The images are stored in TIFF or JPEG format and can be opened in most image processing programs such as Image-Pro Plus and Adobe Photoshop. Since the PC's are connected to the MIT-net, it is easy to transfer data and images to any destination on the internet the user prefers. Alternatively, data and images may be stored on standard floppies, compact discs or Iomega Zip cartridges. Images can also be printed on a 1200dpi Lexmark Optra R⁺ printer.

9.1 The Electron Microprobe at MIT

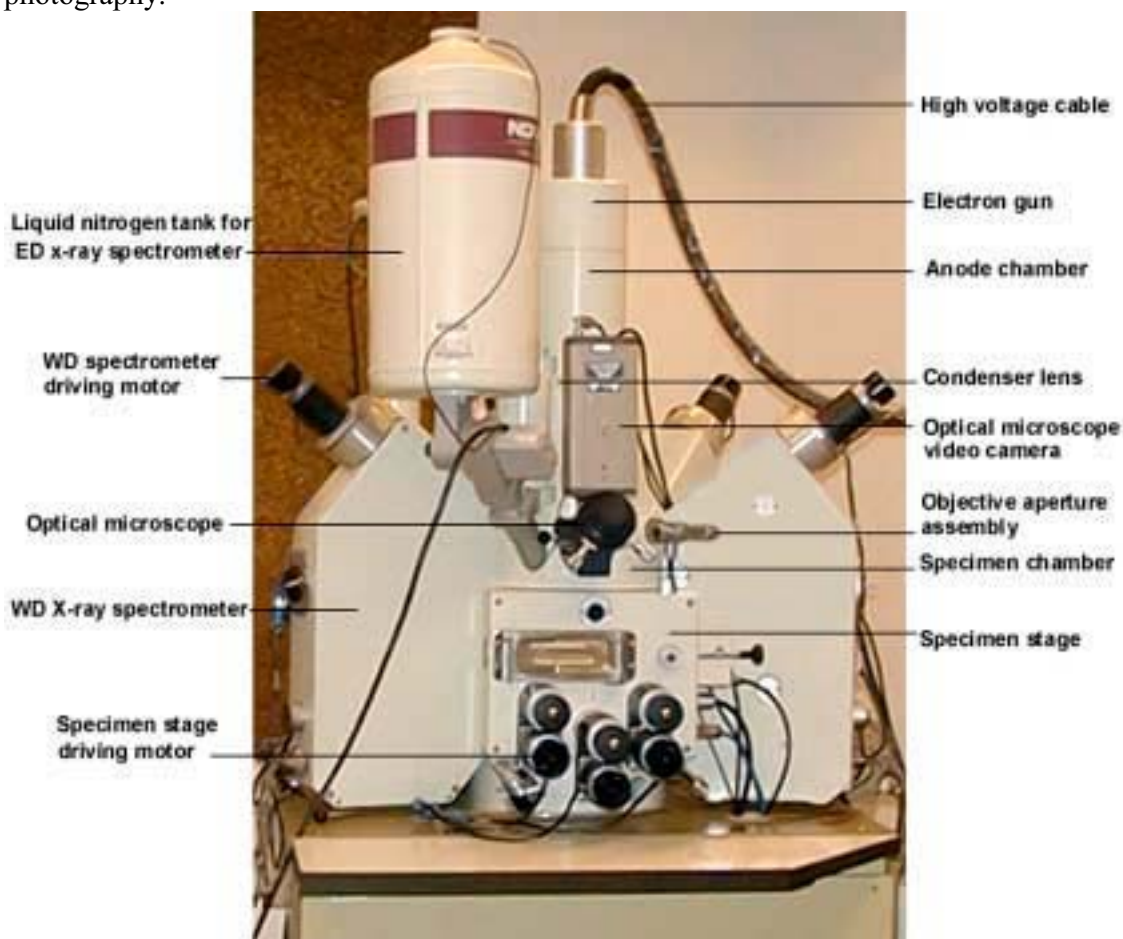
The JEOL JXA-733 Superprobe (the electron microprobe at MIT) has many parts and components. Following is a description of components that are relevant to a regular user:

Electron gun: Emits electrons through thermionic emission from a heated tungsten filament. The gun is a self-biased triode. Accelerating voltages of 1-40 keV is possible, the typical range being 10-20 keV. A saturated filament typically lasts 1-2 months of constant operation. The gun may be aligned by adjusting two pairs of knobs: one for shift correction and the other for tilt correction. There is also an "auto-align/beam-stabilize" feature which keeps the beam aligned and prevents beam current-drift over extended periods.

Electron lenses (condenser and objective): Demagnifies the image of the crossover in the electron gun (10-50 μm) to a final spot on the specimen (1 nm-1 μm , depending on the objective aperture used). Beam currents in the range 1 pA-1 μA is obtained. Typical beam convergence is 1-0.05 $^\circ$. The condenser lens is adjusted to set the beam current (typically 10-100 nA), whereas the objective lens is adjusted to obtain the final beam diameter (typically 0.1-1 μm). The lenses are cooled by circulating oil.

Imaging capability: Backscatter and secondary electron images may be obtained in the range 40-360,000X for compositional imaging and surface study respectively. This is done by rastering the electron beam over a selected area and coupling the signal with that of

an oscilloscope. The image forms on a built-in CRT monitor. The objective and the stigmators are adjusted to obtain a sharp image. The contrast and brightness of an image may be adjusted by adjusting the gain and current in the electron detectors. Image resolution depends on the objective aperture used and the beam current. Elemental x-ray images (dot-maps) may also be obtained by replacing the electron signal with the output from the WDS spectrometers. Sensitivity of an x-ray image decreases at low magnifications as x-rays emitted from a large area cannot be focused into the WDS spectrometers. Two types of image signals may be mixed to obtain a hybrid image. The CRT output may optionally be exposed on a photographic film mounted on a camera attachment for high resolution photography.



Optical Microscope: A reflected light optical microscope is provided to accurately determine the working distance (distance between specimen surface and objective lens). Specimen is viewed and optically focused on a video screen or directly through an eye-piece. The optical focus is used as a standard focussing distance for the electron beam (the image should be focused both on the video screen and on the CRT display) during a quantitative analysis session. A working distance of about 11 mm is used for quantitative analysis. For imaging, it can be increased up to 31 mm to improve depth of focus on uneven surfaces.

EDS spectrometer: Qualitative analysis is normally done using the EDS system fitted with a solid-state Si(Li) detector and a Be window. Elements with atomic number 10 (Na) and higher can be detected. A standardless semi-quantitative analysis may be done on simple compounds (not containing light elements). Quantitative analysis is also possible, but seldom done.

WDS spectrometers: Quantitative analysis is done using these spectrometers. Each WDS spectrometer has a range of delectability (in terms of atomic number) depending upon its diffracting crystal. WDS spectrometry is discussed in detail later.

The vacuum system: The electron gun, the spectrometer column and the sample chamber are kept at a high vacuum to avoid scattering of the electron beam and the emitted x-rays by atmospheric molecules. A diffusion pump, backed by a mechanical rotary pump, is used to maintain a pressure of 2×10^{-5} - 10^{-6} torr; 1 torr being equal to 1 mm of Hg. The atmospheric pressure is approximately 760 mm of Hg at the earth's surface. Thus, the maintained pressure is about one-billionth of the atmospheric pressure. Samples are loaded and unloaded through an airlocking system which precludes the necessity of venting the whole system during these operations.

9.2 A short guide to dQant32 and dPict32

dQant32 and dPict32 are the programs for quantitative analysis and imaging respectively. Following is a brief description and tips for usage of the two programs.

dQant32 operation

dQant32 is the program for quantitative analysis by WDS. It is also the main program from which, Quantum-X (EDS program) and dPict32 can be launched (these two programs can also be started separately). dQant32 consists of setup tables for elements (element table), standards (standard table) and point coordinates (point table), a command field, an output window, a set of control switches and variables, macros to run a batch of commands and the matrix correction subroutines. For details on the menu items and program operation, use online help.

Upon startup, the program shows an output window, different menus and shortcut icons. In the icons bar there is a command field where a command may be typed in. A command may also be executed by choosing an option from the menus (or clicking on an icon or button). The commands executed previously are stored in a buffer and can be accessed by using the scrolling feature associated with the command field. To repeat a command, choose it by scrolling down and click on the arrow on the left of the command field. The program resides in the C:\Program Files\Geller\dQant32\ folder.

Starting dQant32

- 1) From the desktop, double click on the dQant32 icon (top right corner of screen).
- 2) In the command field, type macro `init_rock` (or another `init_macro`) and press Enter to open files and tables. You will be prompted three times to open files. When prompted to open Dataset, just change to your personal folder. You need not worry about filename at this point. The second and third prompts will be to open the Printout file and the Results file. For each of these enter today's date as the filename (e.g., if today is September 6, 2000, enter 090600 as the filename). The filetype should be `txt` for the Printout file and `res` for the Results file.
- 3) If the right Element, Standard and Point tables are not open, click on the Open table icon. If you don't see the file you want, it may be in a different database. Click on the Open file icon, choose a different database and then choose the right table. For silicate analysis, the following files and tables should be open:

o element table:	File: <code>elem1</code>	Table: <code>ELEM1</code>
o standard table:	File: <code>stan2</code>	Table: <code>STAN2</code>
o point table:	File: <code>z</code>	Table: <code>A</code>
- 4) Proceed to calibration and quantitative analysis or other operation.

Quantitative Analysis

Initial steps of a quantitative analysis session are good sample preparation and good alignment and stabilization of the instruments. After samples and standards are loaded, the instrument is calibrated on standards. This involves standard intensity measurement and secondary standard check (sometimes secondary standards may not be available). A 10 μm beam spot size is used for calibration.

- Calibration for standard silicates

The following procedure calibrates for glass, clinopyroxene, orthopyroxene, olivine, plagioclase, spinel, amphibole and all the hydrous silicates:

- 1) Load standard set I.
- 2) Start dQant32 and run macro `init_rock`. Make sure the correct element, standard and point tables are loaded:
 - o File: `elem1`, table: `ELEM1`
 - o File: `stan2`, table: `STAN2` (or `STAN20` for set 2)
 - o File: `z`, table: `A`

Also make sure you open the right Printout file and Results file, both in your personal folder. Follow the standard file naming convention (e.g., if today is May 22, 2000, name your files `052200.txt` and `052200.res`).
- 3) From Macro menu, run macro "cal". You will be asked to check focus on all the standards involved in this calibration.
- 4) Make sure all intensities are reasonable (within 2% of the previous calibration). If not, repeat calibration for the specific element. Type
 - switch focus yes

in command field and press Enter. Next, select the element by bringing the cursor to the extreme left of the element table (when it shows a check mark) and clicking, and then click on the Calibrate button.
- 5) Open Point table "dj35" and focus all points (5) in the table.
- 6) If doing only glass analysis, go to the next step. Otherwise, open tables "alp7", "marj", "synfa", and "lake" and focus all points (5 in each table) in them.
- 7) If doing only glass analysis, run macro "dj_in" and then run macro "dj" on point table "dj35" (see next section). Otherwise, run macro "stds" from the Macro menu.
- 8) Open results file in Excel.
- 9) For each of these standards (dj35, alp7, marj, synfa and lake), calculate average and standard deviations (only dj35, if doing only glass).
- 10) Adjust intensities in element table by typing over the Sinten field of the appropriate element, if necessary. If the actual value lies outside the calculated standard deviation limits of the calculated average of the measured points, the Sinten of that element needs to be adjusted. **BE CAREFUL WHILE EDITING THE TABLE AS THE ORIGINAL VALUES WILL BE PERMANENTLY OVERWRITTEN.** The new value of Sinten for a specific element will be

$$\text{Sinten}_{\text{NEW}} = (\text{average wt}\%_{\text{MEASURED}} / \text{wt}\%_{\text{ACTUAL}}) \text{Sinten}_{\text{OLD}}$$

The following are the elements you should check (you need not be concerned about the other elements):

- o For dj35: Al2, Ca2, Na5, Mg7. *If doing only glass, also do Si2 and Stop here. If doing hydrous glass and analyzing oxygen, calibrate O on Al₂O₃.*
- o For alp7: Si2, Mg2, Fe3
- o For marj: Si1, Mg1
- o For synfa: Fe1
- o For lake: Si5, Al5, Ca5

After you edit Sinten, also change the date field. The date field is reset to a default value every time you change a value in the element table by typing manually.

- Garnet calibration

After you have finished "Calibration for silicate standards", open point tables "kakpyr", "gar87375", "gar110752" and "alman" and focus all points (5 in each table) in them. Then run macros "calgar" and "stdsgar". Open results file, calculate average and standard deviation for each secondary standards and, if necessary, adjust Sinten (as outlined above) as follows:

- For kakpyr: Si6, Mg6, Al6
- For gar110752: Ca6
- For alman: Fe6

- Custom calibration and setup

Individual elements in the element table may be calibrated by bringing the cursor to the extreme left of the element table (when it shows a check mark), clicking, and then clicking on the Calibrate button. Beware of your Control Switch settings. If the Global switch is on along with Stage and Focus, the stage will drive to the position stored in the standard table and ask you to refocus on the standard. If the Focus switch is off, calibration will start immediately without giving you a chance to refocus.

If you are doing a manual calibration, it is advisable to turn off the Stage and Focus switches. Drive to the standard with the joystick, focus and then click on Calibrate. Keep the Global and Background switches on. The Background switch may also be manipulated from the lower right corner of the main window. If you want to measure several point to obtain an average, you may want to switch background off from the second point and use pkCalibrate (which skips the peak search) instead of Calibrate. Make sure the Average Control Switch is on. After measuring the points, open Average Calibration File from the Table menu. Select the points you want to average and click Apply Average.

In the case of prewritten macros such as garnet, check the macro (choose Edit Macro from Macro menu) to determine which elements need to be calibrated. Make sure the standards are loaded in the correct positions. The element table will tell you which standards are needed and standard table will indicate their positions. Run a secondary calibration check, if standards are available. For example, use Kakanui pyrope for pyrope garnet calibration.

If you are writing a new macro, use a preexisting one as a guide and save it under a different name. Also use the corresponding Quant setup file and Results Format file as guides for your new files. If you are doing elemental analysis and in most other cases, edit the Element.mac, Element.qnt and Element.fmt files.

- Running an Analysis Macro

After completing calibration, you can proceed to your sample and select the point you want to analyze. You can analyze one point at a time or analyze a table of stored points in an automated mode.

- Single point analysis

A single point may be analyzed by executing the
Macro *macro_name*
command. If available, run the initialization macro first. For example, run macro "Oliv_in" before running "Olivine".

If an initialization macro is not available, open the appropriate Quant setup table (or create one) and Results format file (or create one). In most cases, while doing elemental analysis (not oxides), edit the Element macro, Element Quant setup file and Element Results format file to suit your needs. Then set the correct number of atoms for stoichiometry calculation and pay attention to the Control Switches and Peak and Background flags in the element table. If you are not sure, keep the Global and Background switches on. The default maximum counting time is 40 seconds. If Global is off, pay attention to the Umax variable in the element table. When Global is on, Background can be turned on or off by clicking the button on the lower right corner of the main window.

- Running a point table

A table of points may be analyzed in an automated mode. In most cases, store your points in table "A" of database file "z". Open this file, delete all points if they exist, and click on Set points, which will prompt you to move the joystick and store points. Points may be deleted by selecting rows and using the Edit menu. All points may be deleted using the Delete all points option of the Edit menu. If you want to do a line scan, store the beginning and end points of the line in the point table and then click on Linescan. A dialog will open asking you to specify the number of points or step size, and the point table you want to store the new points in. In most cases, the new point table would be "Z". If asked to overwrite points, click OK.

After you point table is setup, run the initialization macro. If unavailable, open the required tables and switch on the required switches manually (see last section). Then choose Run on point table from the Macro menu. You will be asked to supply the names of the database file and the table. You may type the command in the command field as follows:

Run point *macro_name table_name database_name*

Features of dQant32

- Printout file

This file stores everything that you see in the output window. Always open your own existing file or create a new one in your folder (\Data\your_name, create your folder from Windows Explorer if it does not exist). If you don't, data will be stored in the file previously opened by the last user. A Printout file can be opened from the File menu of dQant32. You will be prompted to do this when you run one of the init_ macros upon startup.

Printout files are stored as

D:\Data\your_name\filename

where, filename is based on today's date. For example, if today is May 22, 2000, filename should be 052200.txt.

- Results file, Results Format file and Dataset files

The Results file stores only the data part of the output in a delimited text format that can be easily opened in an Excel spreadsheet. The Results Format file specifies which data are to be included in the Results file. This file is usually opened from a macro, but it can be edited to suit the needs of a user in special situations. The Results file, however, should be opened at the beginning of each session. You will be prompted to do this when you run one of the init_ macros upon startup. Otherwise, the data will be stored in a previously opened file.

The Results file may be opened in Excel during a session. But, remember to CLOSE THE RESULT FILE BEFORE YOU ANALYZE YOUR NEXT POINT. Otherwise, the program will attempt and fail to write to an open file. If this happens, you must open the results file again. If you forget to reopen the Results file, the data will no longer be stored in it and the matrix correction subroutine will give an error message.

Fortunately, the program automatically stores the data in smaller files that contain a subset of the data in the Results file. These files, called the Dataset files, are also stored in your folder. The Dataset files include an oxide wt% file (.ox%), an element wt% file (.el%), an atomic proportions file (.ato), a k-ratio file (.kra), a header file (.hdr) and a raw file (.raw). The header file contains information on the matrix correction models being used and the raw file contains count rates, intensities, minimum detection limits and standard deviations for each of the elements being measured.

A Results file can be opened by clicking on the Quant menu and then on the Results File option. You will be prompted automatically to open a Dataset and a Results file when you run one of the init_ macros upon startup. When prompted to open a Dataset file, just change to your folder.

Result files are stored as

D:\Data\your_name\filename

where, filename is based on today's date. For example, if today is May 22, 2000, filename should be 052200.res.

The Dataset files are also stored in your folder as

D:\Data\your_name\macroname.*

where, macroname is the name given to your Dataset files and * stands for ato, el%, ox%, kra, raw and hdr.

Pre-written Results Format files are stored in the Format subfolder of the main program folder.

They have an extension of .FMT. *Custom files may be created in the same folder. In most situations, edit the file Element.FMT.*

- Tips on using Microsoft Access databases

Element, standard and point tables (also, the matrix correction setup tables and Results Format file) reside in Microsoft Access databases. Each row in a table constitutes a record. A field of a record (e.g., Sinten) may be edited through typing. But remember, ANY CHANGE YOU MAKE IN THE TABLE IS PERMANENT. The previous value will be erased as soon as you click on a different row. If you have not clicked on a different row, pressing Esc on the keyboard will restore the original data.

In these tables, one or more rows can be selected with the mouse. Note that the cursor turns to a check mark when it is moved to the extreme left of a record. At this point, if you click the left button of the mouse, the row will be selected. If you want to select another record, hold down the Ctrl key and repeat the last instruction. If you want to select a range of records, use the Shift key instead the Ctrl key. This way you can select the entire table. Alternatively, choose Select entire table from the Edit menu.

Records may be copied or cut and pasted through the edit menu. A new record may be created by scrolling down with the down arrow key after the cursor reaches the last record. A pencil mark appears on the left of the new record indicating that values can be typed into the fields.

You can change the order of the columns by clicking and holding the top of a column and dragging it left or right. You can also resize a column by moving the cursor to a boundary when it changes into two opposing arrows, and dragging the boundary left or right. The records may sorted according to a column by clicking the top of that column.

- Element Table

Element tables contain a list of elements and their analytical setups. A subset of this list is normally used during an analytical session. For each element, the spectrometer (Spec) and crystal (Xtal) assignments are listed, along with standard assignment (Standard), background offsets (High and Low), values for detector bias and PHA baseline and Window, and the unknown maximum counting time (Umax). Background collection and peak search (during quantitative analysis) flags can be enabled or disabled for individual elements. Detector bias, baseline and window settings are determined through SCA scans on the PAC. Note that there may be different reference names for the same element in the element table. These names are associated with different standards. For example, for olivine analysis the Mg1 reference would be used since, Mg1 is calibrated on SYNFO (synthetic forsterite). But for pyroxene analysis, Mg2 would be used since it is calibrated on ALP7 (synthetic aluminous orthopyroxene).

Element tables also contain regularly updated values for peak position (Pos) standard intensities (Sinten), and background intensity (Sbkg). These values are updated in the course of a calibration process. Peak position is in terms of the L-value (in mm), or the distance between the beam impact point on the sample and the analyzing crystal, which is directly proportional to wavelength of the x-ray being detected. A new element reference may be set up by typing in the different fields of the newly created record.

The Element table contains buttons such as Calibrate, pkCalibrate and Measure. This can be used to calibrate or measure specific elements. Calibration is done standards, whereas, Measure is used for unknowns. PkCalibrate calibrates an element without performing a peak search.

Element tables created for specific purposes are as follows:

Database file: elem1	Table: ELEM1	<i>Purpose</i>
	Sulfide	<i>silicate analysis</i>
	Carbonate	<i>sulfide analysis</i>
	Element	<i>carbonate analysis</i>
		<i>all other analyses</i>

- Standard Table

Standard tables contain a list of standards, their last stored coordinates (X, Y and Z, in mm) on the stage and their composition. If the Stage Control switch is on, the stage will automatically drive to the stored positions during calibration, or when the Get Element button is clicked. The table contains other buttons such as Focus and Set. Clicking on any of these buttons invokes a dialog window through which the user can jog the stage, go to a different point, put the cup in or out and store the current coordinates of the stage. Focus is used to renew the coordinates of a standard after the stage drives to its current position. While using the Set button, the stage remains in its current position. In this case, the usual practice is to turn on the image, locate the point, focus on it, and then store the position.

Standard tables created for specific purposes are as follows:

Database file: stan1	Table: STAN2	<i>Purpose</i>
	STAN20	<i>standard set I</i>
	Sulfide	<i>standard set II</i>
	Carbonate	<i>sulfide standards</i>
	Element	<i>carbonate standards</i>
		<i>all other standards</i>

- Point Table

Point tables contain X, Y, and Z coordinates of points stored by the user, which may be called in for automated analyses. A point table also contains buttons similar to the standard table, which can be used in a similar way.

Point tables created for specific purposes are as follows:

Database file: z	Table: A	<i>Purpose</i>
	Z	<i>general purpose</i>
	Linescan	<i>linescan and other purpose</i>
	Dj35	<i>creating a linescan</i>
	Alp7	<i>secondary check</i>
	Marj	<i>secondary check</i>
	Synfa	<i>secondary check</i>
	Lake	<i>secondary check</i>

Kakpyr, Gar87375, Gar110752, Alman, Alvin 1690-20, Glass 70-002 and Hydr-gls are also for *secondary check*

- Control Switches

The control switches are usually handled by the Analysis Macros and an average user should not be concerned with them.

A set of switches through which, the user can set up the program for different automated tasks. The control switches are accessible through the Options menu of dQant32. The most important switch is the Global switch. If this switch is not turned on, it disables all the other switches. The other important switches are Background and Scan which enables background measurement and peak searching on unknowns. When the Global switch is on, all the elements being measured through a command line are treated the same way. For example, background will be measured on all the elements if the Background switch is turned on. If you want to selective background measurements and peak searches, turn off the Global switch and turn on only the switches for the desired elements in the element table.

- Control Variables

The control variables usually don't require any change and an average user should not be concerned with them.

A set of variables through which, the user can set up the minimum and maximum counting times, the standard deviation requirements for measurement, peak search parameters, warning message control and other parameters. Some of them work only when the Global Control Switch is on.

- Analysis Macros

Analysis Macros are batch files of commands that are used conveniently to open specific files and setups and analyze certain types of compounds. *Advanced users may be able to save their own setup files and write their own Analysis Macros.* But several macros and setups have been developed in this lab over the years to analyze certain silicates such as olivines, pyroxenes, amphiboles, feldspars and glass.

For each mineral there are two macros. The first macro initializes different parameters and loads the right tables. It also switches on background measurement. The filename for this macro ends with `_in`. This macro is run once, every time the user wants to analyze several points on a particular phase or mineral. The user may also want run it if a re-initialization is desired, for example, if background measurement is necessary. After the initialization macro is executed, the main analysis macro may be run as many times as desired. Below are examples of an initialization macro and a main macro:

Initialization macro for olivine (Oliv_in.mac):

```

open format olivine                                opens the olivine Results Format file
open quant olivine                                  opens the matrix correction setup file for olivine
zaf model heinrich                                  selects the Heinrich model for matrix correction
zaf atoms -4                                        sets the oxygen atoms to 4 for stoichiometry calculation
switch global no                                    switches Global Control Switch off
peak mg1 yes al2 no si1 yes mn4 no fe1 yes ca2 no ti4 no cr6 no
                                                    sets peak search switches for each element in element table
bkg mg1 yes al2 yes si1 yes mn4 yes fe1 yes ca2 yes ti4 yes cr6 yes
                                                    sets background switches for each element in element table
umax mg1 40 al2 40 si1 20 mn4 40 fe1 20 ni1 40 ca2 40 ti4 40 cr6 40
                                                    sets the maximum counting time for each element
next 1                                              sets analysis number to 1
label                                              prompts for a sample label

```

Main analysis macro for olivine (Olivine.mac):

```

get element Mg1 Al2 Mn4 Ca2                        moves spectrometers to the desired elements
measure mg1 al2 si1 mn4 fe1 ni1 ca2 ti4 cr6        measures counts for each element for time specified in umax
bkg mg1 no al2 no si1 no mn4 no fe1 no ni1 no ca2 no ti4 no cr6 no
                                                    sets background measurement off for each element
quant olivine                                       applies matrix correction and prints out concentrations

```

Pre-written Analysis Macros are stored in the Macro\mineral\ subfolder of the main program folder. They have an extension of `.mac`. *Custom files may be created in the same folder. In most situations, edit the files `elem_in.mac` and `element.mac`.*

- Setup Files for matrix correction

This table is loaded from the macro and an average user should not be concerned with it.

Quant setup files are a table of elements or their oxides, which are measured by the macro and whose accumulated counts will be used to calculate their concentrations. Each entry has an elemental reference, which correspond to the element table. This in turn links the elemental reference to the standard composition specified in the standard table. The x-ray line being measured is specified and the composition of the standard is entered from the standard table.

In the ZAF setup (in the Options menu), the number of anions (e.g., oxygen atoms) or cations for stoichiometry calculations and the matrix correction model to be used can be set.

Pre-written Quant Setup files are stored in the Quant subfolder of the main program folder. They have an extension of .qnt. *Custom files may be created in the same folder. In most situations, edit the file element.qnt.*

- Shortcut keys

A number of shortcut keys (e.g., Ctrl+, Alt+, etc.) for different functions are specified in a reference table. This table can be opened from the Options menu. *An advanced user can create his own shortcut key table and load it every time at the beginning of his session.* The default file for silicate analysis is Silicate.fky.

Important shortcuts are Ctrl+F1 through Ctrl+F7 which drive the stage to positions 1 through 7 on the main sample holder. F8 can be used to drive to the sample change coordinates.

dPict32 operation

dPict32 is the program for acquiring digital scanning images including backscattered electron, secondary electron, cathodoluminescence and elemental x-ray by WDS and EDS. Large area mapping is possible through mosaic imaging. In this method, many images are acquired and tiled to create a large mosaic image. The size of each tile can be set. Once an image is acquired, limited image processing like adjusting the brightness and contrast of the image can be done through dPict32. The image can also be printed on a 1200dpi printer.

Acquiring a simple image

Following are the steps involved in acquiring an image:

- 1) Drive stage to the area of the sample to be imaged.
- 2) With SEI pressed, turn on OM and focus on the sample.
- 3) Turn off OM and press the appropriate image selector switch.
- 4) Turn Scan Generator knob to Bright Up Positioning.
- 5) Press EXT and then CUP to extinguish the LED's on these buttons.
- 6) Press Rapid 3 scanning speed and zoom in or out on the image.
- 7) Make sure image is in focus (See Locating and looking at a sample).
- 8) Double-click on dPict32 icon on the desktop screen, or on dQuant32 task bar.
- 9) From Acquire menu, select Setup an image.
- 10) In the dialog window, change to your personal folder (\Image\your_name, create your folder from Windows Explorer if it does not exist).
- 11) Select the appropriate signal sources on the left-hand column. The first source is whatever you selected on the CRT (SEI or COMPO). The ROI's correspond to EDS (See Quantum-X operation). To collect EDS x-ray images, the EDS spectrum must be set to acquire the entire time. Disable preset time in EDS and click on Acquire.
- 12) Type in filename, label caption, filename-tag and caption prefix. Each image will be saved in a separate file.

- 13) Set the number of pixels between 500 and 750, and the dwell time between 0.1 and 5 msec. More pixels and longer dwell time increases the image acquisition time. If collecting only a scanning electron image, a dwell time of 0.1-0.3 is sufficient.
- 14) Set the magnification to whatever magnification is displayed on the CRT. This will make sure that the scale bar on the acquired image is accurate. For WDS x-ray images, the minimum magnification should be 600X. Lower magnifications lead to imaging artifacts on WDS x-ray images.
- 15) Click OK.
- 16) After the images are acquired, save all images.
- 17) Close dPict32 by clicking on the cross on the top right of the main window.

Acquiring a mosaic image

A mosaic image may be acquired in a similar way. Steps 1-8 are the same as above. Following are the other steps involved:

- 9) From Acquire menu, select Setup mosaic image.
- 10) In the dialog window, change to your personal folder (`\Image\your_name`, create your folder from Windows Explorer if it does not exist).
- 11) Select the appropriate signal sources on the left-hand column. The first source is whatever you selected on the CRT (SEI or COMPO). The ROI's correspond to EDS (See Quantum-X operation). To collect EDS x-ray images, the EDS spectrum must be set to acquire the entire time. Disable preset time in EDS and click on Acquire.
- 12) Type in filename, label caption, filename-tag and caption prefix. Each image will be saved in a separate file.
- 13) Click OK. You will see another dialog appear.
- 14) Drive stage to the top left corner of the area to be imaged. Click on the appropriate box to set the coordinates. Also drive stage to the lower right corner and set its coordinates. The top right corner only sets the Z coordinate and used to maintain focus over the whole area.
- 15) Set the number of pixels between 1000 and 2000, and the dwell time between 0.1 and 5 msec. More pixels and longer dwell time increases the image acquisition time. If collecting only a scanning electron image, a dwell time of 0.1-0.3 is sufficient.
- 16) Set the magnification to whatever magnification is displayed on the CRT. For WDS x-ray images, the minimum magnification should be 600X. Lower magnifications lead to imaging artifacts on WDS x-ray images.
- 17) Check number of tiles in the X and Y directions and the estimated time. Click OK if you are satisfied. If not, reset the top left and lower right coordinates. You may also start acquiring the image and then abort it, if you think the estimated time is too long. Discard the partially acquired image and go back to the Setup mosaic image dialog. The dialog retains your previous inputs, so you can make only the necessary corrections.
- 18) After the images are acquired, save all images.
- 19) Close dPict32 by clicking on the cross on the top right of the main window.